Host Contact Structure is Important for the Recurrence of Influenza A

by

Juan M. Jaramillo
B.Sc., University of Victoria, 2015

A Thesis Submitted in Partial Fulfillment of the
Requirements for the Degree of

MASTER OF SCIENCE

in the Department of Mathematics and Statistics

Host Contact Structure is Important for the Recurrence of Influenza A

by

Juan M. Jaramillo
B.Sc., University of Victoria, 2015

Supervisory Committee

Dr. J. Ma, Co-supervisor
(Department of Mathematics and Statistics)

Dr. P. van den Driessche, Co-supervisor
(Department of Mathematics and Statistics)

Supervisory Committee

Dr. J. Ma, Co-supervisor
(Department of Mathematics and Statistics)

Dr. P. van den Driessche, Co-supervisor
(Department of Mathematics and Statistics)

ABSTRACT

An important characteristic of influenza A is its ability to escape host immunity through antigenic drift. A novel influenza A strain that causes a pandemic confers full immunity to infected individuals, yet because of antigenic drift, these individuals have decreased immunity to drifted strains. We compute the required decrease in immunity so that a recurrence is possible. Models for influenza A must make assumptions on the host contact structure on which the disease spreads. By computing the reproduction number, we show that the classical random mixing assumption predicts an unrealistically large decrease of immunity before a recurrence is possible. We improve over the classical random mixing assumption by incorporating a contact network structure. A complication of contact networks is correlations induced by the initial pandemic. Thus, we provide a novel analytic derivation of such correlations and show that contact networks may require a dramatically smaller drop in immunity before recurrence. Hence, the key new insight is that on contact networks the establishment of a new strain is possible for much higher immunity levels of previously infected individuals than predicted by the commonly used random mixing assumption. This suggests that stable contacts like classmates, coworkers and family members are a crucial path for the spread of influenza in human population.

Contents

List of Tables

List of Figures

ACKNOWLEDGEMENTS

I would like to thank:

the math faculty at UVic, for the high quality math lectures delivered with invaluable nuggets of life wisdom.

My supervisors, for their patience, counsel, and inspiration to pursue excellence.

Friends, for providing an outlet from work and countless outdoor adventures.

My family, for their encouragement and unyielding support; to whom I owe this work.

Chapter 1

Introduction

Seasonal influenza is an acute viral infection that is highly infectious and circulates worldwide. It is commonly referred to as 'the flu'. There are three main types (A, B, C) of seasonal influenza viruses, however, types A and B are most responsible for outbreaks and pandemics in humans. Influenza A viruses are further classified by subtypes according to the combination of two surface proteins, haemagglutinin (HA) and neuraminidase (NA). The subtypes of influenza A virus currently in circulation are A(H3N2) and A(H1N1)pdm09 [2]. Influenza spreads readily among individuals via infectious droplets dispersed by sneezing, coughing or conversation [13]. Influenza poses a significant social and economic burden; annually, the global number of cases may be in the order of a billion, resulting in 250,000-500,000 deaths [1]. Furthermore, the high morbidity rate gives rise to a high loss of economic productivity due to worker absenteeism [2].

The topic of this thesis the influenza type A virus. An important feature of this virus is its relative fast-scaled evolution. In fact, significant evolution is thought to occur in the time-scale of a couple of years [9, 16]. This is important for public health considerations since although an individual infected with a particular strain recovers with complete protection one season, the virus may evolve to re-infect the same individual in following influenza seasons. The evolution responsible for this takes place as a modification to antigenic surface HA and NA proteins [7]. These modifications prevent specialized host antibodies from detecting the virus; effectively allowing the virus to re-infect a host with full acquired immunity to the previous form of the virus. [9, 32].

There a two generally accepted mechanisms for the modification of antigenic HA and NA proteins. The first is commonly referred to as antigenic shift, and is a

sudden, and dramatic change caused by combination and re-assortment of genetic material from distinct and co-circulating influenza strains. Shifts, although relatively rare and random events, are of high concern since they often give rise to large scale pandemics [9]. Such examples include the notorious 1918 Spanish flu that resulted in an estimated 20-50 million deaths world-wide [33], and more recently, the 2009 H1N1 pandemic [2].

The second mechanism is referred to as antigenic drift; a more subtle mechanism acting by way of frequent, point mutations at the antigenic sites of the virus; allowing the strain to drift away from recognition by the host's immune system. These point mutations are thought to occur while replicating, and while some mutations may be neutral in that they do not affect the binding from host antibodies to the proteins, others may negatively affect such binding. When this type of mutation happens, a natural selection process leads to its survival and establishment among the human population [9].

The two-fold evolutionary process gives way to a two-fold epidemiological phenomenon in which first, a novel and highly virulent influenza subtype emerges as a result of antigenic shift, causes a pandemic, and through antigenic drift remains as a re-curring seasonal subtype until challenged by a novel subtype [5]. In fact, at the time of writing this thesis, all circulating influenza viruses are drift products of previous pandemic influenza strains [2, 9]. Figure 1.1 gives a graphical representation of the aforementioned phenomenon.

Developing models for the spread and evolution of Influenza A has been a rich topic for mathematical epidemiology and ecology. Generally, the goal has been to test and develop control measures for influenza epidemics and to fundamentally capture many of the characteristics associated with influenza A. Such characteristics include but are not limited to seasonality, coexistence or replacement of subtypes and the coupled drifting and immunity dynamics. Most of these models have built upon the fundamental Kermack-McKendrick SIR compartmental (or 'box') model [20]. An early example is done by Pease in 1987 [31]. This model made the assumption that a dominant virus strain is present every season. Furthermore, it simplified the evolutionary process of influenza A by assuming that influenza variants may be ordered on a one dimensional axis and that a constant antigenic drift moved the current strain along the axis. The model exhibited damped oscillations with periods of approximately the right interval of time between epidemics caused by the same influenza subtype [3]. By coupling evolutionary dynamics with epidemiological ones, some

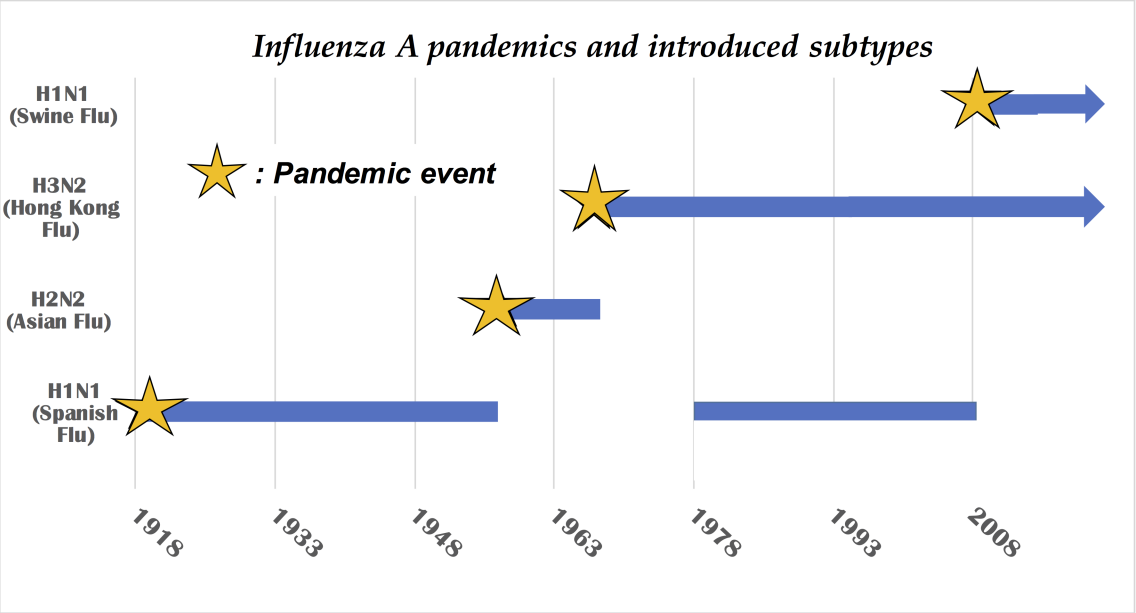

Figure 1.1: Pandemics have resulted from new subtypes following antigenic shift events. Following the pandemic, the subtypes may remain as drifted variants that cause seasonal epidemics. In the last hundred years, the pandemic events that have occurred and introduced seasonal subtypes include: 1918 Spanish flu, 1957 Asian flu (H2N2), 1968 Hong Kong flu (H3N2), and the 2009 Swine flu (H1N1pmd09). Variants of the 1968 H3N2 and 2009 H1N1 pandemic remain in circulation today as seasonal strains.

models do not make the constant antigenic drift assumption. For example, Boni et al. [6] studied the interplay between epidemic sizes and population immunity. While a larger epidemic increases the rate of antigenic drift, it also gives partial immunity to a larger fraction of individuals the virus must overcome the following year. Results in [6] strengthened the case for mass vaccination as it protects the population through classical herd immunity and reduced the rate of antigenic drift season to season. In addition, they showed that a disease with a fast evolution rate will always be able to invade susceptible populations.

As mentioned, other models have considered the dynamics involved when multiple influenza strains are simultaneously present. These models, exhibit complex behaviour and they inherently require demographic considerations such as birth and deaths for the long-term co-existence of multiple strains [4]. In addition [5] investigates conditions where replacement or co-existence occurs at the introduction of a novel pandemic subtype.

The models discussed above have not only provided important insights into the spread of influenza A, but have also provided a mathematical framework on which

to further study other hypotheses. However, an assumption common to the models discussed and many others is that of a randomly mixing population. Most of the models just discussed make the assumption of random mixing; where as the name suggests, individuals in a population are randomly mixing. This assumption is discussed more in depth in Chapter 2. Here it suffices to say that this assumption may not be appropriate for modelling influenza. In fact, most interactions an infectious individual has could occur within a fixed set of contacts. We are effectively describing a social network. From this point of view, a disease such as influenza A is transmitted only if two individuals are contacts.

There has been a rapidly growing body of evidence that suggests that in the real social network, disease dynamics may differ significantly from those made by the random and proportionate mixing assumptions [11, 15, 24, 30]. Specifically, there are differences in values of epidemiological interest for infectious diseases such as the final size, or $\mathcal{R}_0$, the basic reproduction number (see Chapter 2). Motivated by the difference between random mixing and network models, the goal of this paper is to explore how incorporating a structure that mimics a real social network may invoke further insight in the context of influenza A. Specifically, we study the amount of influenza drift necessary for a novel pandemic subtype to become seasonal on a contact network-type structure and compare these results to the classical random mixing assumption. This leads to our key new insight: on a social network, considerably less antigenic evolution may be required for the endemic establishment of a novel pandemic subtype.

1.1 The biological assumptions

In this thesis we use the framework provided by Andreasen in [3], where the time scale within and between influenza seasons are separated. Furthermore as in [3], we assume that there is a dominant strain responsible for the majority of infections in each influenza season. Effectively, this means that individuals infected during the pandemic wave develop complete immunity for the remainder of the pandemic event but, due to antigenic drift, will only have partial immunity to the drifted strain in the following season. This means that antigenic drift results in an increase in susceptibility among recovered individuals but does not change infectivity or the infectious period. Therefore, for the remainder of this thesis, we use antigenic drift, an increase in susceptibility, and a drop in immunity interchangeably.

In our models we do not incorporate demographic effects due to the difference in time scales. Furthermore, since the number of influenza induced deaths is a small fraction of those infected [33], deaths due to influenza A are ignored.

Finally, in this thesis, 'first wave' and 'pandemic event' are used interchangeably as well as the 'second wave' or 'recurrence event.' We note that in literature, authors sometimes refer to the first and second wave to describe inter-pandemic spikes-usually a few months apart; this is not to be confused with our usage here where the second wave only occurs a period of time after the pandemic event has fully ran its course.

1.2 Thesis structure

Chapter 2 provides a background on basic mathematical epidemiological theory including a review of classical epidemiological SIR models and modern contact network SIR models. Chapters 3 and 4 contain the bulk of the novel work. Specifically, Chapter 3 builds upon the results of Chapter 2 to model the pandemic and first return of the pandemic subtype using random mixing models. Furthermore, basic reproduction numbers for the second wave ($\mathcal{R}_0^{(2)}$) are compared as a function of the amount of antigenic drift between the pandemic and first return of the same subtype. Chapter 4 is structured just as Chapter 3, except that we assume a contact network type population structure. Finally, a discussion of the significance and limitations of the results of Chapters 3 and 4 are provided in Chapter 5, followed by concluding remarks.

Chapter 2

A background on mathematical epidemiology theory

Before the main results in Chapter 3 and 4, we provide a brief introduction to mathematical epidemiology theory. Since the thesis mainly deals with ordinary differential equations (ODE) models, we limit the introduction to the classical random mixing and network ODE models. We also opt to present the material in the most illuminating way for Chapter 3 and 4 as possible. For a more in depth review of mathematical epidemiology, [8] is an excellent resource.

2.1 Classical compartmental disease models

The goal of infectious disease models is usually to track the number of individuals infected by some disease. Thus, a natural model formulation is to divide a population into compartments based on their disease status or a characteristic relevant to the dynamics for the disease in question. The transfer of individuals between compartments will be based on the disease and assumptions on the rate of movements of individuals between compartments. All the models we focus on will be such that the size of the compartments are differentiable with respect to time. Thus, the transfer of individuals between compartments can be written as a system of ordinary differential equations (ODEs).

Implicit in the models given in this section is the random mixing assumption. This is the assumption that individuals within a compartment are indistinguishable, and that if two compartments have nonzero interaction rates, then any individual from one

compartment may interact with any individual in the other compartment. In other words, any infectious individual may transmit the disease to any given susceptible individual.

2.1.1 The Kermack and McKendrick SIR model

The first compartmental disease models were introduced in a 1927 paper by Kermack and McKendrick [20]. The simplest of these models is the well studied SIR model describing the flow between the fraction of susceptible (S), infectious (I), and recovered individuals (R).

$$S' = -\tilde{\beta}SI \tag{2.1}$$

$$I' = \tilde{\beta}SI - \gamma I \tag{2.2}$$

$$R' = \gamma I \tag{2.3}$$

Here $\tilde{\beta}$ and γ are the transmission and recovery rates, respectively. Note that by ignoring demographic effects, $S + I + R = 1$. Typical initial conditions where there are a few infectious individuals to begin with are:

$$S(0) \approx 1 \tag{2.4}$$

$$I(0) \approx 0 \tag{2.5}$$

$$R(0) = 0 \tag{2.6}$$

For the remainder of the thesis, we refer to this model as the 'homogeneous' SIR model. Before presenting some analytical results, we introduce another more general random mixing model.

2.1.2 Multigroup model

If the underlying population is not homogeneous, then incorporating heterogeneities has been found to be important [18, 30]. Instead of initially lumping the entire population into a single susceptible compartment, the number of compartments is increased to reflect this heterogeneity. The generalized SIR multigroup model with demographics 'switched off' and M distinct subpopulations is constructed following

the framework in [18]:

$$S_k' = -kS_k \sum_{\ell=1}^{M} \beta_{k\ell} I_\ell \tag{2.7}$$

$$I_k' = kS_k \sum_{\ell=1}^{M} \beta_{k\ell} I_\ell - \gamma_k I_k \tag{2.8}$$

$$R_k' = \gamma_k I_k, \text{ for } k = 0, 1, 2, ..., M \tag{2.9}$$

Here, β_{ki} is the per capita transmission rate from an infectious member in population i to one in population k. Furthermore, γ_k represents the recovery rate for a member of population k.

For the purposes of this thesis, the heterogeneity occurs only in the average number of contacts per unit time. Thus the model has compartments $\{S_k, I_k, R_k\}$ for k ranging from one to the maximum rate of contacts, M per unit time. Note that in this thesis we use $X_k \in \{S_k, I_k, R_k\}$ to refer to both the compartment and fraction of individuals belonging to this compartment. Furthermore, we assume that there is a fixed number of individuals in each contact class and that transmission rates are proportional the number of contacts per unit time. Thus $p_k = S_k + I_k + R_k$ gives the fraction of all individuals with k contacts. For an individual in S_k, a proportion $(\sum jI_j / \sum jp_j)$ of the k contacts per unit time lead to disease transmission, and the rate leaving S_k is thus $\beta k S_k (\sum jI_j / \sum jp_j)$. The proportion $(\sum jI_j / \sum jp_j)$ comes from the fact that in a well mixed population, the probability of encountering an individual that makes on average a higher number of contacts is higher than one with a lesser amount of contacts. That is to say, the probability of randomly encountering an individual is proportionate to not only their density, but also the number of contacts they in turn make. Analogous to the SIS model in [30], the SIR model is given by the system:

$$S_k' = -\beta k S_k \frac{\sum_{\ell=1}^{M} \ell I_\ell}{\sum_{\ell=1}^{M} \ell p_\ell} \tag{2.10}$$

$$I_k' = \beta k S_k \frac{\sum_{\ell=1}^{M} \ell I_\ell}{\sum_{\ell=1}^{M} \ell p_\ell} - \gamma I_k \tag{2.11}$$

$$R_k' = \gamma I_k, \text{ for } k = 0, 1, 2, ..., M \tag{2.12}$$

along with initial conditions

$$S_k(0) \approx p_k \tag{2.13}$$

$$I_k(0) \approx p_k - S_k(0) \tag{2.14}$$

$$R_k = 0 \tag{2.15}$$

Since this is a closed system, the population is constant and $\sum_k S_k + I_k + R_k = 1$.

2.2 Basic reproduction number $\mathcal{R}_0$

The basic reproduction number $\mathcal{R}_0$ is an important epidemiological value defined as the expected number of new infections caused by a single infectious individual introduced into a completely susceptible population. If $\mathcal{R}_0 < 1$, then on average, a single infected individual will not spread the disease to others and the disease will die out without a significant increase in newly infectious individuals. If $\mathcal{R}_0 > 1$, the first few infectious individuals will on average infect one or more individuals so that the disease initially propagates resulting in an outbreak.

For the homogeneous SIR model, the expression for $\mathcal{R}_0$ is very well known.

Theorem 1. *[8] For the homogeneous SIR model given in Section 2.1.1,* $\mathcal{R}_0 = \frac{\tilde{\beta}}{\gamma}$

To see why this should be true, note that with the introduction of a few infectious individuals, an epidemic will only occur if $\tilde{\beta}SI - \gamma I > 0$, or equivalently, if $\tilde{\beta}S > \gamma$. Recalling that $S(0) \approx 1$ and simplifying gives the required result.

For more complicated ODE models, $\mathcal{R}_0$ is rigorously defined as the spectral radius of the next generation matrix (NGM) evaluated at the disease free equilibrium (DFE)[36]. For example, in the homogeneous SIR model, $S = 1$, $I = 0$, $R = 0$ is the DFE. We now state the following fundamental theorem that applies to most disease models of ODEs.

Theorem 2. *[36] Assuming a standard epidemiological disease that satisfies conditions in [36],* $\mathcal{R}_0$ *is the spectral radius of the NGM evaluated at the DFE. Furthermore the DFE is locally asymptotically stable when* $\mathcal{R}_0 < 1$ *and unstable when* $\mathcal{R}_0 > 1$.

We direct the interested reader to [36] for the proof, instead we illustrate its application for the multigroup SIR model. First, we turn our attention to compartments that involve infectious individuals, namely $\{I_1, I_2..., I_M\}$. We rewrite equation 2.11 as

$$I_i' = \mathcal{F}_i - \mathcal{V}_i$$

where $\mathcal{F}_i$ represents terms resulting from new infections, namely $\mathcal{F}_i = \beta k S_k \frac{\sum_\ell \ell I_\ell}{\sum_\ell \ell p_\ell}$ and $\mathcal{V}_i$ captures terms involving disease progression including recovery. Thus, $\mathcal{V}_i = \gamma I_i$. Next, we take partial derivatives with respect to $\{I_1, I_2..., I_M\}$ and evaluate at the DFE:

$$F = \begin{pmatrix} \frac{\beta p_1}{\sum \ell p_\ell} & \frac{\beta p_1}{\sum \ell_\ell} & \cdots & \frac{\beta M p_1}{\sum \ell p_\ell} \\ \frac{\beta 2 p_2}{\sum \ell p_\ell} & \frac{\beta 2^2 p_2}{\sum \ell p_\ell} & \cdots & \frac{\beta 2 M p_2}{\sum \ell p_\ell} \\ \vdots & \vdots & & \vdots \\ \frac{\beta M p_M}{\sum \ell p_\ell} & \frac{\beta 2 M p_M}{\sum \ell p_\ell} & \cdots & \frac{\beta M^2 p_M}{\sum \ell p_\ell} \end{pmatrix} \vdots, \; V = \gamma I_{M \times M}$$

Finally, FV^{-1} gives the NGM. Note that $rank(FV^{-1}) = 1$ since $rank(F) = 1$ and so the spectral radius is equal to the sum of diagonal entries.

Theorem 3. *[14] For the multigroup SIR with contact heterogeneity described in Section 2.1.2,*

$$\mathcal{R}_0^{(1)} = \frac{\beta}{\gamma} \frac{\sum_k k^2 p_k}{\langle k \rangle} = \frac{\beta}{\gamma} \left(\frac{Var[k]}{\langle k \rangle} + \langle k \rangle \right)$$

This shows how for the multigroup model with heterogeneity in the number of contacts, $\mathcal{R}_0^{(1)}$ is related to the variance and expected value for the number of contacts per unit time, as observed in [14].

2.3 Final size relations

We've established that if $\mathcal{R}_0^{(1)} > 1$, then the introduction of a few infectious individuals will result in an epidemic, and the progression of individuals through disease states is often described by a system of non-linear ODEs. Thus, epidemiologically important parameters such as the final size (i.e., the fraction of individuals that contract influenza A in the first wave) would require formidable computational power. However, as we show next, it is often possible to derive final size equation(s), whose solution(s) determine the final size and other parameters of interest for an epidemic.

2.3.1 Final size for the homogeneous SIR model

We begin by calculating a well-known expression for the final size given by the homogeneous SIR model.

Theorem 4. *[8] For the homogeneous SIR with $\mathcal{R}_0 > 1$, the final size of the epidemic is given by $1 - S_\infty$ where S_∞ is the unique solution in $[0, 1)$ to*

$$S_\infty = e^{-\mathcal{R}_0(1-S_\infty)} \tag{2.16}$$

Moreover, if $\mathcal{R}_0 < 1$ then $S_\infty = 1$ is the only solution in $[0, 1]$; corresponding to the case there is no epidemic.

We provide a brief calculation to illustrate the process for arriving at Theorem 4. Begin by dividing equation 2.1 by S, integrating both sides from 0 to ∞

$$\begin{aligned} ln(S_\infty) - ln(S(0)) &= -\int_0^\infty \tilde{\beta} I \\ ln(S_\infty) &= -\frac{\tilde{\beta}}{\gamma} R\Big|_0^\infty \text{ using 2.3 and } S(0) \approx 1 \\ ln(S_\infty) &= -\frac{\tilde{\beta}}{\gamma}(R(\infty)) \text{ from } R(0) = 0 \end{aligned}$$

Finally, using relations $R_\infty = 1 - S_\infty$ and Theorem 1 gives (2.16). Note that $S_\infty = 1$ is always a solution corresponding to the case that there is no epidemic. To illustrate the utility of a final size-type equation, suppose that at the beginning of an outbreak it is estimated that $\mathcal{R}_0 \approx 2$, then estimating the total number of individuals that will be infected is equivalent to finding the unique point of intersection between $[0, 1)$ for the functions $f(x) = x$ and $g(x) = e^{-2(1-x)}$. Thus, an important epidemiological quantity was calculated without the need to numerically solve a non-linear system of ODEs. As shown in Figure 2.1 (a), $S_\infty \approx 0.2032$ is the non-trivial solution. Thus, the homogeneous SIR model predicts that approximately 79.68% of the population will be infected. If however, $\mathcal{R}_0 < 1$ then $S_\infty = 1$ is the only solution in $[0, 1]$ as illustrated by Figure 2.1 (b). Of course, this corresponds to the scenario where there is no epidemic.

2.3.2 Final size for multigroup SIR model

It is also possible to derive the final size for the multigroup SIR model given by (2.10)-(2.15). For convenience, we express the distribution of individuals in contact

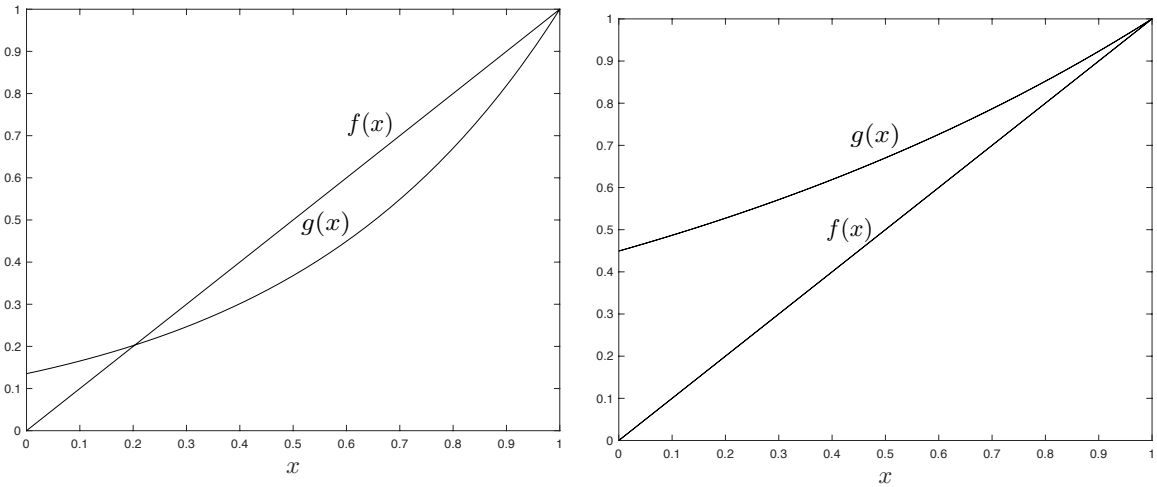

(a) (b)

Figure 2.1: The two possible geometric regimes for the intersection of $g(x) = e^{-\mathcal{R}_0(1-x)}$ and $f(x) = x$ in $[0, 1]$. S_∞ is equal to the value for the smallest point of intersection in [0,1]. In Figure 2.1 (a) $\mathcal{R}_0 = 2$, while for Figure 2.1 (b) $\mathcal{R}_0 = 0.8$.

rate classes using a probability generating function (PGF)

$$\psi(x) = \sum_{k=1}^{M} p_k x^k$$

where p_k is as defined in Section 2.1.2. Note that a PGF is a convenient way of encoding a probability distribution since for example, for the the mean $\langle k \rangle$,

$$\langle k \rangle = \sum_{k=1}^{M} k p_k = \psi'(1)$$

Theorem 5. *For the multigroup model given by (2.10)-(2.15)* $S_\infty = \psi(\theta_\infty)$*, where* θ_∞ *is smallest solution in* $[0, 1]$ *to the equation*

$$\theta_\infty = \exp\{-\frac{\beta}{\gamma}\left(1 - \frac{\theta_\infty \Psi'(\theta_\infty)}{\Psi'(1)}\right)\} \tag{2.17}$$

Proof. The equation for S_k' is linear in S_k and so the solution has general form $S_k(t) = S_k(0) \exp\{-\int_0^t \beta k \frac{\sum_\ell \ell I_\ell}{\sum_\ell \ell p_\ell} dt\}$. Defining

$$\theta(t) = \exp\{-\int_0^t \beta \frac{\sum_\ell \ell I_\ell}{\sum_\ell \ell p_\ell} dt\} \tag{2.18}$$

gives

$$S_k(t) = S_k(0)\theta(t)^k$$

Thus, to obtain the final size of each compartment it is sufficient to calculate

$\lim_{t\to\infty}\theta_t = \theta_\infty$. Integrating (2.12) gives

$$\int_0^\infty I_k dt = \frac{1}{\gamma}R_k(\infty) = \frac{1}{\gamma}(p_k - S_k(\infty)) = \frac{1}{\gamma}p_k(1-\theta_\infty^k)$$

Substituting into (2.18) and simplifying gives the result. Finally a concavity and monoticity argument omitted here shows that (2.17) has at most two roots in [0,1], with one of them always equal to 1. Furthermore, it can be shown that the second root only appears when $\mathcal{R}_0 > 1$. □

We note that this result is also provided in [21].

2.4 Background: network models

2.4.1 Configuration Model networks

Fixed contact networks are graphs in which nodes and edges represent individuals and contacts among individuals, respectively. Determining exact contact networks for a large population is not a feasible task, however, network statistics such as size and degree probability distributions may be determined; see, for example, [34]. With the degree probability distribution, networks can be generated via the 1995 Molley and Reed algorithm [29]. A very brief description of the algorithm is as follows. Assign to each node in a collection of edgeless nodes, a degree drawn from a given degree probability distribution. For the degree drawn, attach this number of half edges or 'stubs' to each node. Then choose two stubs uniformly and connect them to make an edge. We note that the sum of total degrees may not be even and/or loops may be possible in this construction; degrees may be re-drawn to fix the parity and loops are eliminated. Networks produced by this algorithm are generally referred to as Configuration Model (CM) networks and have the prescribed degree distribution, negligible clustering and negligible degree correlations. It is important to note that following a random edge from any given node, the probability of arriving at a node of a given degree is not only proportional to the density of such nodes in the network but also to the degree (i.e., densities being equal, it is more likely to arrive at higher degree nodes than lower degree nodes). This is in fact consistent with the real-world phenomenon where 'your friends have more friends than you do' [17]. Deterministic models of SIS and SIR type disease spread on CM networks have been developed; see, for example, [15, 24, 37, 29, 25]. Most of these models were derived from seemingly different vantage points, differ in complexity, and differ in the physical quantities they

track during an epidemic, however they are intrinsically related and in some cases equivalent; see for example, [19, 26, 35]. It is important to keep in mind that for all of the models just discussed, nodes or individuals undergo changes only in labelling, that is, individuals change in status as it relates to the disease states, however, the underlying contact network is assumed to stay fixed throughout the entire process.

For the remainder of this chapter, we assume that a Configuration Model network is given and it has a degree distribution with PGF:

$$\Psi(x) = \sum_k p_k x^k$$

2.5 Pairwise SIR Model

The first model we introduce is the pairwise SIR model [19]. This was a natural extension of an SIS model first introduced by Eames and Keeling in [15].

Let β be the transmission rate across an edge and γ be the recovery rate for an infectious node. Denote S_k as the fraction of nodes in the network that are of degree k and susceptible. These nodes stop belonging to S_k when transmission occurs across an edge. The rate at which this happens is $\beta[S_k I]$ where as the notation suggests, $[S_k I]$ is the fraction of edges leaving a node in S_k and leading to an infectious neighbour of any degree (i.e., $\sum_j [S_k I_j]$). There is an inherent order assigned when writing $[S_k I]$ versus $[I S_k]$ however, the number of edges in both classes are the same and thus only the dynamics for one is required. Therefore,

$$\frac{d}{dt} S_k = -\beta [S_k I] \tag{2.19}$$

The dynamical equation for the $[S_k I_j]$ compartment is now required. Consider an edge in $[S_k I_j]$. It leaves $[S_k I_j]$ when either

1. the infectious node in I_j transmits along the edge to S_k; or
2. the node in I_j recovers; or
3. another neighbour of the S_k node is infectious and transmits to the S_k node.

Furthermore, an edge in $[S_k S_j]$ enters $[S_k I_j]$ when transmission occurs through another neighbour of the node in S_j. The need to consider neighbours outside of the $[S_k I_j]$ pair requires the use of triples $[S_k S_j I]$ and $[I_j S_k I]$. Thus, writing the evolution

equation for $[S_kI_j]$ in the order described gives

$$\frac{d}{dt}[S_kI_j] = -\beta[S_kI_j] - \gamma[S_kI_j] - \beta[I_jS_kI] + \beta[S_kS_jI]$$

The evolution equation for $[S_kS_j]$ is arrived at in a similar fashion to give

$$\frac{d}{dt}[S_kS_j] = -\beta([S_kS_jI] + [S_jS_kI])$$

Although we have written the dynamical equations for the pairs used in this model, these depend on triples. Thus a full model would provide the dynamics for triples, that would in turn depend on quadruples; obviously dimensionality and complexity of such a model would grow rapidly. Instead, a closure scheme that estimates the number of triples in terms of pairs is used [19]. If X_j and Y_k are disease state classes, the triple closure scheme used is

$$[X_jY_kI] \approx \frac{[X_jY_k][Y_kI](k-1)}{kY_k} \tag{2.20}$$

Utilizing these in the equations involving triples above, gives the full system given in [19]:

$$\frac{d}{dt}[S_kI_j] = -\beta[S_kI_j] + \beta\frac{[S_kS_j][S_jI](j-1)}{jS_j} - \beta\frac{[IS_k][S_kI_j](k-1)}{kS_k} - \gamma[S_kI_j] \tag{2.21}$$

$$\frac{d}{dt}[S_kS_j] = -\beta\left(\frac{[S_kS_j][S_jI](j-1)}{jS_j} + \frac{[IS_k][S_kSj](k-1)}{kS_k}\right) \tag{2.22}$$

$$\frac{d}{dt}[S_kR_j] = \gamma[S_kI_j] - \beta\left(\frac{[IS_k][S_kR_j](k-1)}{kS_k}\right) \tag{2.23}$$

$$\frac{d}{dt}S_k = -\beta[S_kI] \tag{2.24}$$

Assuming that initial infectious contacts are uniformly distributed among all degree classes, the initial conditions are as follows:

$$[S_kI_j](0) = kS_k(0)\frac{I_j(0)}{\psi'(1))} = kp_k(1-\pi)\frac{\pi jp_j}{\psi'(1)} \tag{2.25}$$

$$[S_kS_j](0) = kS_k(0)\frac{jS_j(0)}{\psi'(1)} = kp_k(1-\pi)^2\frac{jp_j}{\psi'(1)} \tag{2.26}$$

$$[S_kR_j](0) = 0 \tag{2.27}$$

$$S_k(0) = p_k(1-\pi), \tag{2.28}$$

where $0 < \pi \ll 1$, is the probability a given node is infectious at time 0.

The pairwise model has been accepted as a flexible framework and good starting point for modeling infectious processes on a network. However, the number of equa-

tions scale up proportionally to N^2, where N is the highest degree of the network; making analytical work difficult and numerical results computationally expensive. Thus, we turn to the low dimensional yet, powerful edge based compartmental model (EBCM) for SIR-type diseases on a network.

2.6 Edge Based Compartmental Models

2.6.1 Introduction

In 2008, Volz [37] introduced the edge-based compartmental model (EBCM) to describe SIR dynamics on a configuration model random network. This was a non-linear system of differential equations that did not scale up with the highest degree found in the network and it numerically performed well against full stochastic simulations. In a 2011 paper by Miller [25] a simpler system composed of a single ODE equation and equivalent to the Volz model was introduced.Furthermore, as proven in [26] and in Appendix A, the EBCM and SIR pairwise models turn out to be equivalent under mild assumptions on the initial conditions. In this section we introduce the Miller-Volz model as presented in [25].

2.6.2 Derivation

The probability that an individual with k contacts remains susceptible by time t is the probability that the disease has not been transmitted across any of its k edges. We define $\theta(t)$ as the probability that there has not been infectious transmission across an edge towards the given individual by time t. Recall that a random network generated by the configuration model has negligible clustering and therefore transmission across edges are independent events so that the probability a degree k node is susceptible at time t is θ^k.

We define ϕ as the fraction of edges leading to a susceptible node and also connected to an infectious node at time t. Note that these edges are also in θ. Thus,

$$\frac{d}{dt}\theta = -\beta\phi \tag{2.29}$$

The dynamical equations for ϕ are required. We let $h(t)$ be the probability the node reached following a θ edge (out of the S node) has not been infected at time t. A node reached by following a θ edge is in S_j with probability $\frac{jp_j}{\Psi'(1)}\theta^{j-1}$. Note that

θ is raised to the power $j-1$ to account for the fact that transmission cannot occur across the followed θ edge. Summing over j gives

$$h(t) = \sum_j \frac{j p_j \theta^{j-1}}{\psi'(1)} \tag{2.30}$$

$$= \frac{\psi'(\theta)}{\psi'(1)} \tag{2.31}$$

The rate at which edges enter ϕ, is equal in magnitude to the rate at which neighbors reached by following a θ edge become infectious. Thus, ϕ is increased at a rate $-\frac{d}{dt}h(t)$. The equation for ϕ is then,

$$\frac{d}{dt}\phi = -(\beta+\gamma)\phi - \frac{d}{dt}h(t)$$

The equations for ϕ can now be written as

$$\frac{d}{dt}\phi = -(\beta+\gamma)\phi - \frac{d}{dt}h(t) \tag{2.32}$$

$$= -(\beta+\gamma)\phi - \frac{\psi''(\theta)}{\psi'(1)}\theta' \tag{2.33}$$

$$= -(\beta+\gamma)\phi + \beta\frac{\psi''(\theta)}{\psi'(1)}\phi \tag{2.34}$$

The equation for $\frac{d}{dt}\phi$ can be integrated using (2.29) and initial conditions $\theta(0) \approx 1$, $\phi(0) \approx 0$ giving

$$\phi(t) = (1+\frac{\gamma}{\beta})(\theta-1) - \frac{\psi'(\theta)}{\psi'(1)} + 1 \tag{2.35}$$

The dynamical equations for θ and ϕ drive the dynamics of the system, however since the variable of interest are the number of susceptible and infectious individuals we augment these equations with

$$S = \sum_k p_k \theta^k = \psi(\theta) \tag{2.36}$$

$$I = 1 - S - R \tag{2.37}$$

$$\frac{dR}{dt} = -\gamma I \tag{2.38}$$

For SIR disease dynamics on a Configuration Model random network, the basic

reproduction number for the first wave is given by [24, 25, 29, 37]

$$\mathcal{R}_0 = \left(\frac{\beta}{\beta+\gamma}\right)\frac{\psi''(1)}{\psi'(1)} \tag{2.39}$$

The term $\frac{\beta}{\beta+\gamma}$ is the probability for transmission before recovery, and $\frac{\psi''(1)}{\psi'(1)}$ is referred to as the average excess degree. i.e., the degree of a node found by following a random edge minus one for the edge being followed. Thus, the product gives the average number of new neighbours infected by an individual reached via an edge.

2.6.3 Final size equation

Just like there is the simple final size equation for the homogeneous SIR model as given by Theorem 4, it is possible to derive a simple relation that describes the final size of a SIR epidemic on a Configuration Model network. From (2.36), it follows that calculating the final size reduces to the problem of finding the final state $\theta_\infty \in (0,1)$ for θ. Solving the equilibrium condition for (2.29) or equivalently, solving $\phi(t) = 0$ using (2.35) leads to the equilibrium condition for θ_∞

$$\theta_\infty = \frac{\gamma}{\beta+\gamma} + \left(\frac{\beta}{\beta+\gamma}\right)\frac{\Psi'(\theta_\infty)}{\Psi'(1)} \tag{2.40}$$

Heuristically, following an edge from a randomly selected susceptible node, it remains in θ by time t if the neighbour node reached did not have a transmission event across it while it was infectious. The probability of a transmission event before recovery is $\frac{\beta}{\beta+\gamma}$. Let $h(t)$ be the probability the neighbour node is susceptible given that we have followed an edge leaving a susceptible node. Note that this $h(t)$ is as in (2.31). It follows that $1-h(t)$ is the probability the neighbour node has been infectious at some point in the past and we can write

$$\theta(t) = 1 - \frac{\beta}{\beta+\gamma}(1-h(t))$$

Taking the limit as $t \to \infty$ gives the required result.

Finally, using (2.40), the final size of the epidemic is given by

$$1 - S_\infty = 1 - \Psi(\theta_\infty)$$

2.6.4 Equivalence with SIR pairwise model

In [26], it is shown that if the initially infectious individuals are uniformly chosen among all degree classes, for example as described by (2.25)-(2.28), then the SIR pairwise model and SIR edge based compartmental basic SIR model are equivalent. For completeness, we provide a proof in Appendix A.

Chapter 3

Random mixing models for the recurrence of influenza A

3.1 Introduction

In Chapter 1 we discussed the observed phenomenon of seasonal establishment following an initial pandemic due to a novel influenza A subtype. Since this is a well documented epidemiological pattern for influenza, it is worthwhile to develop mathematical models that predict this phenomenon. In this chapter we establish that random mixing models predict relatively high levels of antigenic drift is required for a recurrence of influenza A.

3.2 Homogeneous model

3.2.1 First wave dynamics

The first wave is described by the classic Kermack-McKendrick SIR model given by equations (2.1)-(2.3) along with initial conditions (2.4)-(2.6). As discussed in chapter 2, the first wave basic reproduction number $\mathcal{R}_0^{(1)}$ is given by the ratio $\frac{\tilde{\beta}}{\gamma}$. Furthermore, the fraction that escaped the pandemic S_∞ is the solution in $(0, 1)$ to equation (2.16).

3.2.2 Second wave dynamics

For the second wave caused by the drifted pandemic subtype, individuals recovered from the first wave are partially susceptible to the drifted strain with susceptibility

$\sigma \in [0,1]$. Of course, the values $\sigma = 0$ and $\sigma = 1$ correspond to no and full susceptibility, respectively. The fraction of these individuals is denoted by A, and the initial conditions are $A(0) \approx 1 - S_\infty$, $S(0) \approx S_\infty$, $I(0) \approx 0$, $R(0) = 0$. The SAIR dynamics are given by the equations

$$\begin{aligned} S' &= -\tilde{\beta} SI \\ A' &= -\sigma \tilde{\beta} AI \\ I' &= (\tilde{\beta} S + \sigma \tilde{\beta} A)I - \gamma I \\ R' &= \gamma I \end{aligned}$$

The reproduction number for the second wave is $\mathcal{R}_0^{(2)} = \frac{\tilde{\beta}}{\gamma}(S(0) + \sigma A(0))$, which may be reformulated using $\mathcal{R}_0^{(1)} = \frac{\tilde{\beta}}{\gamma}$ as

$$\mathcal{R}_0^{(2)} = \mathcal{R}_0^{(1)} S_\infty + \sigma \mathcal{R}_0^{(1)}(1 - S_\infty) \tag{3.1}$$

where S_∞ is given numerically by (2.16). This expression for $\mathcal{R}_0^{(2)}$ depends linearly on σ.

For example, if $\mathcal{R}_0^{(1)} = 2$, then $\mathcal{R}_0^{(2)} > 1$ for $\sigma > 0.37$ (i.e., an outbreak is possible for susceptibility greater than 0.37). This gives susceptibility threshold, $\sigma_T \approx 0.37$. Thus, in order for a recurrence to be possible, the virus must undergo significant antigenic drift before it may cause another epidemic. This is larger than the observed value of $\sigma_T \approx 0.25$ for influenza A(H3N2) [23]; see also [22].

3.3 Multigroup SIR model

Now we model the first wave and second using a multigroup type approach as introduced in Section 2.1.2. Let p_k denote the proportion of individuals with k daily contacts, and for convenience we use the probability generating function (PGF) formalism, $\Psi(x) = \sum_k p_k x^k$ to represent the probability distribution for the rate of contacts.

3.3.1 First wave dynamics

The equations which describe the first wave are given by (2.10)-(2.12) with initial conditions (2.13)-(2.15). Theorem 3 gives an equation for $\mathcal{R}_0^{(1)}$ and Theorem 5 pro-

vides an expression for the final size that can be solved numerically. The final state is then used to the parametrize the second wave SAIR multigroup model.

3.3.2 Second wave dynamics

We extend the first wave model in a straightforward manner to include the individuals who were infected and recovered in the pandemic wave while keeping their heterogeneity in contact rates. We denote the fraction of degree k individuals that were previously infected as A_k, and define σ as before.

$$\begin{aligned} S_k' &= -\beta k S_k \frac{\sum_\ell \ell I_\ell}{\sum_\ell \ell p_\ell} \\ A_k' &= -\sigma\beta k A_k \frac{\sum_\ell \ell I_\ell}{\sum_\ell \ell p_\ell} \\ I_k' &= \beta k(\sigma A_k + S_k)\frac{\sum_\ell \ell I_\ell}{\sum_\ell \ell p_\ell} - \gamma I_k \\ R_k' &= \gamma I_k, \text{ for } k = 0, 1, 2, ..., M \end{aligned}$$

The initial conditions are $S_k(0) \approx p_k\theta_\infty^k$, $A_k(0) = p_k(1-\theta_\infty^k)$, $I_k(0) \approx 0$, $R_k(0) = 0$. The next generation matrix approach gives

$$\mathcal{R}_0^{(2)} = \frac{\beta}{\gamma}\frac{\sum_k((\sigma A_k(0) + S_k(0))k^2)}{\langle k\rangle}$$

This can be rewritten in terms of θ_∞ as

$$\mathcal{R}_0^{(2)} = \frac{\beta}{\gamma}\frac{\sum_k(\sigma(1-\theta_\infty^k) + \theta_\infty^k)p_k k^2}{\langle k\rangle} \tag{3.2}$$

where θ_∞ is found by solving (2.17). Thus, once again, $\mathcal{R}_0^{(2)}$ is linearly dependent on σ. Before presenting the numerical results for this chapter we highlight the special cases when $\mathcal{R}_0^{(1)}$ is very large and small. When $\mathcal{R}_0^{(1)} \to \infty$, Theorem 4 and Theorem 5 predict that $S_\infty \to 0$. Thus, (3.1) and (3.2) show that $\mathcal{R}_0^{(2)} \to \sigma\mathcal{R}_0^{(1)}$. Therefore, increasing $\mathcal{R}_0^{(1)}$ leads to a smaller σ_T value. For $\mathcal{R}_0^{(1)} \to 1^+$, $S_\infty \to 1$ so $\mathcal{R}_0^{(2)} \to \mathcal{R}_0^{(1)}$ regardless of σ.

The threshold value σ_T for the multigroup model is found numerically for a given PGF $\Psi(x)$ and fixed $\mathcal{R}_0^{(1)}$. For all simulations in this section, we choose a time scale so that

$\gamma = 1$, and parametrize commonly used distributions so that average excess degree is 3, 5 and 10 (or equivalently, $\frac{\langle k^2 \rangle}{\langle k \rangle} = 4, 6, 11$ respectively; see Appendix D). Notice that this means that β must be specified by the desired value of $\mathcal{R}_0^{(1)}$. Figure 3.1 shows how introducing heterogeneity in contact rates decreases the susceptibility threshold. However, such decrease is modest; for example, at $\mathcal{R}_0^{(1)} = 2$ (approximately the value of $\mathcal{R}_0$ for the 1918 Spanish flu pandemic [27]), the multigroup model equipped with a power law distribution for contact rates predicts that $\sigma_T \approx 0.33$ while for the homogeneous model, $\sigma_T \approx 0.37$. Finally, we have found numerically that as $\frac{\langle k^2 \rangle}{\langle k \rangle}$ increases, the multigroup lines approach the homogeneous mixing line as shown by Figure 3.1

Furthermore, to illustrate that these results are not only valid for $\mathcal{R}_0^{(1)} = 2$, we provide Figure 3.2 to show how values for the susceptibility threshold (σ_T) change for a range of $\mathcal{R}_0^{(1)}$ values. Although increasing $\mathcal{R}_0^{(1)}$ results in lower σ_T values, all the multigroup and homogeneous models decrease at around the same rate.

Thus, in this chapter we have shown that the random mixing assumption requires relatively high levels of antigenic drift that do not seem to reflect estimated values [22, 23], where antigenic evolution in the time scale of a few years has been modest ($\sigma_T \approx 0.25$) [23]. This suggests that random mixing models may be unsuitable for modelling pandemic influenza, and we turn our attention to contact network structures.

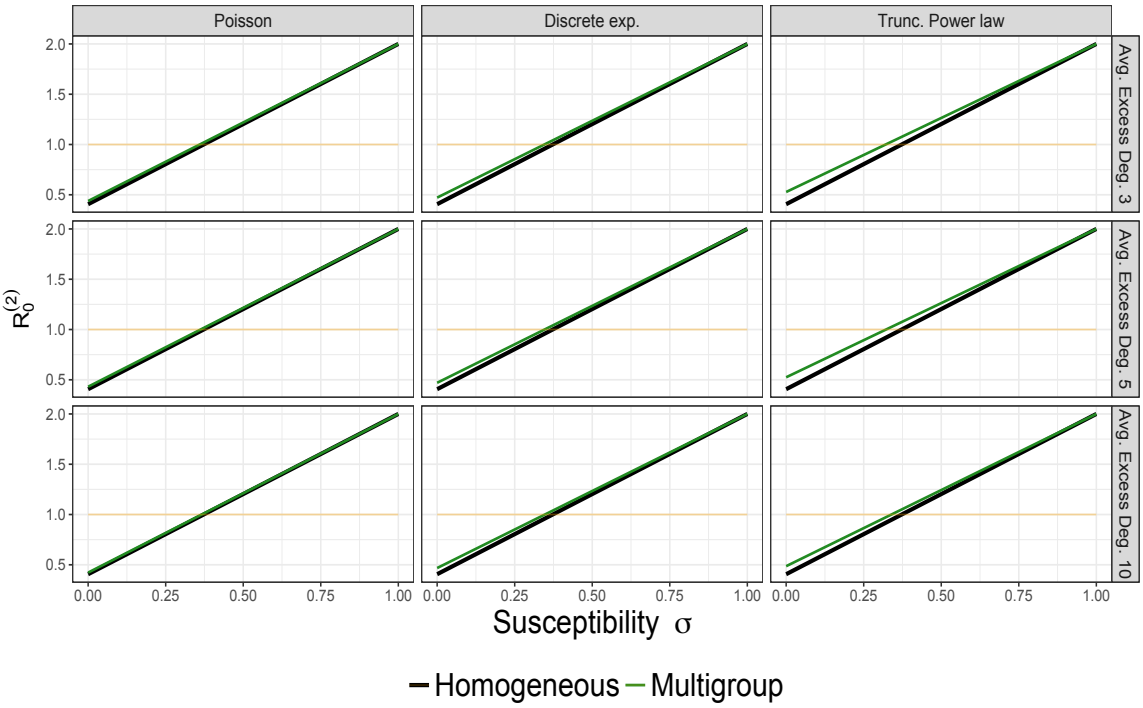

(a)

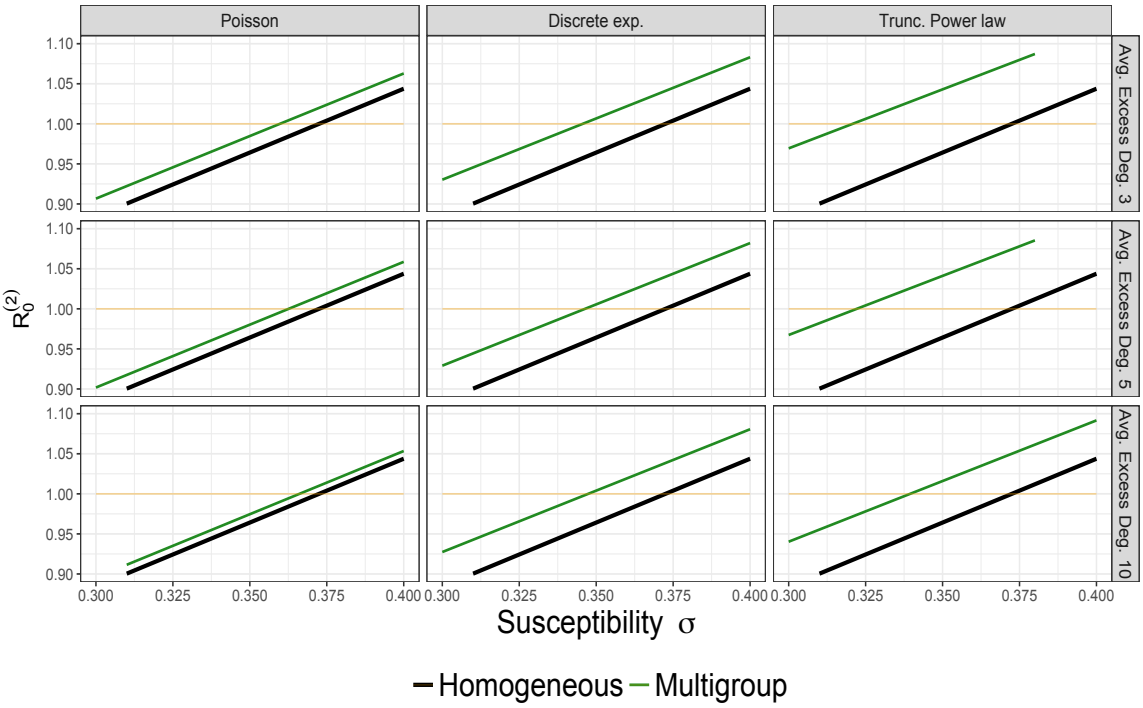

(b)

Figure 3.1: In Figure 3.1 (a) we plot $\mathcal{R}_0^{(2)}$ vs. σ. Modest decreases in σ_T occur when heterogeneity is included using multigroup models. For these results, $\mathcal{R}_0^{(1)} = 2$ and a timescale is chosen so that $\gamma = 1$. In Figure 3.1 (b), we have enlarged the plots in Figure 2.1 (a) around the threshold $\mathcal{R}_0^{(2)} = 1$. For all distributions considered, the multigroup model slightly decreases σ_T. For a complete description of the probability distributions considered see Appendix D.

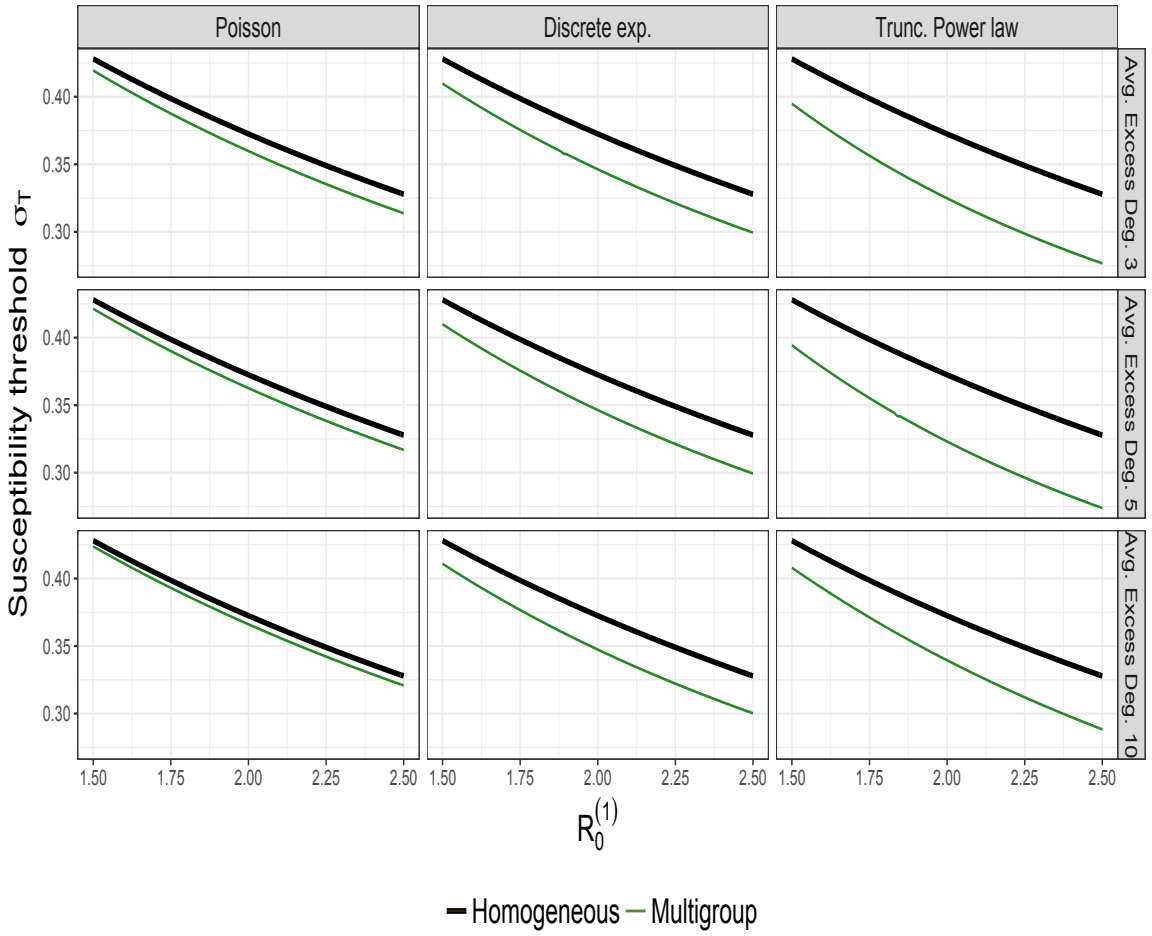

Figure 3.2: Here, σ_T vs. $\mathcal{R}_0^{(1)}$ is compared among all distributions outlined in Appendix D. It is clear from these plots that the results shown in Figure 3.1 are expected to be robust for a range of likely values of $\mathcal{R}_0^{(1)}$ for the pandemic event.

Chapter 4

Modelling two waves of influenza A with a contact network model

4.1 Introduction & first wave dynamics

In chapter 3 we determined that for random mixing models high levels of antigenic drift are required for the return of influenza A following a pandemic. Thus, in this chapter we compare these results to those when influenza A spreads on a contact network. For the first wave dynamics, we assume the network is a Configuration Model network with degree PGF $\Psi(x) = \sum_k p_k x^k$ and employ the pairwise SIR model given by equations (2.21)-(2.24) and initial conditions (2.25)-(2.28). As discussed in Chapter 2, the first wave basic reproduction number is given by

$$\mathcal{R}_0^{(1)} = \left(\frac{\beta}{\beta+\gamma}\right)\left(\frac{\psi''(1)}{\psi'(1)}\right) \tag{4.1}$$

The final size of the pandemic is given by $R_\infty = 1-\Psi(\theta_\infty)$ where θ_∞ is found by solving equation (2.40). However, the final size for the pandemic wave does not provide the complete network configuration. Specifically, pair-type correlations induced by the disease dynamics need to be incorporated.

4.2 The final state of the first wave

In the homogeneous mixing case, only the final state for the variables S (S_k) in the homogeneous (multigroup) model respectively are required for the second wave model.

In Chapter 2, we supplied the final state for S_k nodes, however there is no known expression for the final state at the level of pairs.

Recall that the pairwise SIR model simplifies to the Miller model under the initial conditions (2.25)-(2.27). To derive the complete final state of the system we begin with the conservation of mass equations:

$$\begin{aligned}[N_kN_j] =&[S_kS_j](t) + [S_kI_j](t) + [I_kS_j](t) + [I_kI_j](t) + [S_kR_j](t) + [R_kS_j](t) + [I_kR_j](t)+\\ &+ [R_kI_j](t) + [R_kR_j](t)\end{aligned}$$

Since we are only concerned with state of the variables at the end of the first epidemic when there are no infectious individuals remaining and thus no pairs involving infectious nodes. The conservation of mass equations in the limit simplify to

$$[N_kN_j](\infty) = [S_kS_j](\infty) + [S_kR_j](\infty) + [R_kS_j](\infty) + [R_kR_j](\infty)$$

The fraction of $[N_kN_j]$ pairs is determined from the Configuration Model framework. Specifically,

$$[N_kN_j] = \frac{(kp_k)(jp_j)}{\psi'(1)} \tag{4.2}$$

Furthermore, Appendix A gives an expression for $[S_kS_j](t)$ in terms of θ and other known parameters. Specifically,

$$[S_kS_j](t) = \frac{(kp_k)(jp_j)}{\psi'(1)}\theta^{k+j-2} \tag{4.3}$$

where θ is given by (2.29). Furthermore, we will need the following results from Appendix A;

$$\theta_k = e^{-\beta\int_0^t P_{I|S_k}d\tau}$$

and

$$\theta_k = \theta_\ell$$

for any ℓ, k. Thus, we will drop the subscript and simply use θ. Note that since θ_∞ can easily be determined by using (2.40), $[S_kS_j](\infty)$ follows. Note that if we had $[S_kR_j](\infty)$ in terms of θ_∞ and other known parameters, then by the conservation of mass equation, we have $[R_jR_k](\infty)$ (since $[S_jR_k](\infty)$ follows immediately from $[S_kR_j](\infty)$ by symmetry). This idea is illustrated by the flow diagram given in Figure 4.1.

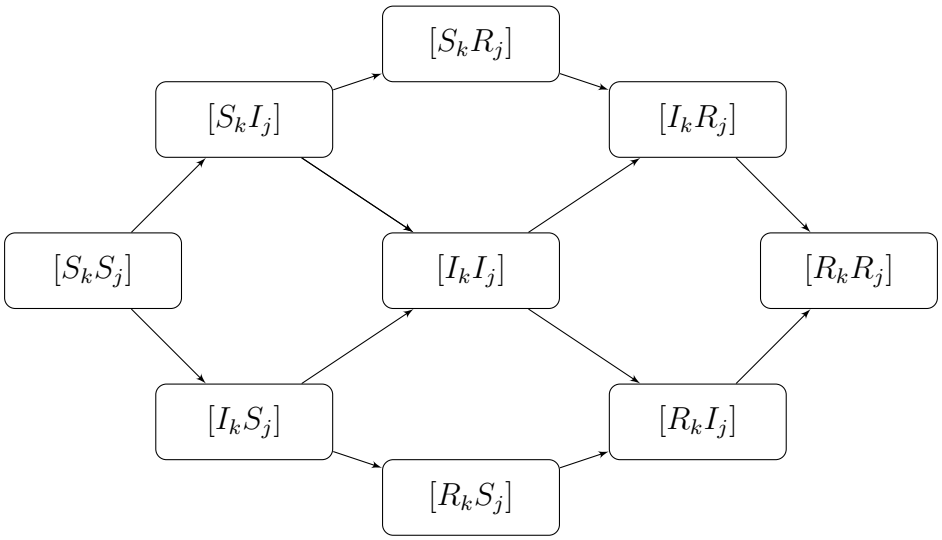

Figure 4.1: The possible transitions for the pair $[X_kY_j]$. As the first wave dies out or equivalently, as $t \to \infty$, the only compartments remaining are those where $X, Y \in \{S, R\}$. An expression for each of these four compartments in terms of θ_∞ is derived in Section 2.1.2.

Our starting point to obtain $[S_kR_j](\infty)$ is the differential equation for $[S_kI_j]$ given by (2.21) and initial condition (2.25). Defining $P_{I|S_j} := \frac{[S_jI]}{jS_j}$, and substituting into (2.21) gives

$$\frac{d}{dt}[S_kI_j] = \beta[S_kS_j]P_{I|S_j}(j-1) - [S_kI_j](\gamma+\beta) - \beta P_{I|S_k}[S_kI_j](k-1)$$

multiplying by an integrating factor and simplifying yields

$$\frac{d}{dt}\left([S_kI_j]e^{\int_0^t\left((\beta+\gamma)+\beta P_{I|S_k}(k-1)\right)d\tau}\right) = \beta[S_kS_j]P_{I|S_j}(j-1)e^{\int_0^t\left((\beta+\gamma)+\beta P_{I|S_k}(k-1)\right)d\tau}$$

which is integrated and simplified to yield

$$\begin{aligned}[S_kI_j](t) &= \left(\int_0^t \beta[S_kS_j](a)P_{I|S_j}(a)(j-1)\theta^{-(k-1)}(a)e^{(\beta+\gamma)a}da\right)\theta^{k-1}e^{-t(\beta+\gamma)} \\ &\quad + [S_kI_j](0)\theta^{k-1}e^{-t(\beta+\gamma)} \qquad (4.4) \\ &= \left(\int_0^t \beta(\frac{p_kp_jjk(j-1)\theta(a)^{k+j-2}}{\langle k\rangle})P_{I|S_j}(a)e^{(\beta+\gamma)a}\theta(a)^{-(k-1)}da\right)\theta^{k-1}e^{-t(\beta+\gamma)} \\ &\quad + [S_kI_j](0)\theta^{k-1}e^{-t(\beta+\gamma)} \qquad (4.5)\end{aligned}$$

$$= (\frac{p_k p_j kj}{\langle k \rangle}) \left(\left(\int_0^t \beta(j-1) P_{I|S_j} \theta(a)^{j-1} e^{(\beta+\gamma)a} da \right) + c[S_k I_j](0) \right) \theta(t)^{k-1} e^{-(\beta+\gamma)t}$$
$$= (\frac{p_k p_j kj}{\langle k \rangle}) \left(\left(\int_0^t -\frac{d}{da} \left(\theta(a)^{j-1} \right) e^{(\beta+\gamma)a} da \right) + c[S_k I_j](0) \right) \theta(t)^{k-1} e^{-(\beta+\gamma)t} \quad (4.6)$$

where

$$c = \left(\frac{p_k p_j kj}{\langle k \rangle} \right)^{-1}$$

At this point we leave the current expression for $[S_k I_j](t)$ and turn to calculate $[S_k R_j](t)$. Recall that

$$\frac{d}{dt}[S_k R_j](t) = \gamma[S_k I_j] - \beta[S_k R_j] P_{I|S_k}(k-1)$$

multiplying out by an integrating factor gives

$$\frac{d}{dt} \left([S_k R_j](t) e^{\int_0^t \beta P_{I|S_k}(k-1)} \right) = \gamma[S_k I_j] e^{\int_0^t \beta P_{I|S_k}(k-1)} = \gamma[S_k I_j] \theta^{-(k-1)}$$

Integrating,

$$[S_k R_j](t) = \gamma \left(\int_0^t [S_k I_j](\tau) \theta^{-(k-1)}(\tau) d\tau \right) \theta^{(k-1)}(t)$$

Substituting (4.6) gives

$$[S_k R_j](t) = \gamma (\frac{p_k p_j jk}{\langle k \rangle}) \left(\int_0^t F_j(\tau) e^{-(\beta+\gamma)\tau} d\tau \right) \theta^{(k-1)}(t)$$

where

$$F_j(\tau) := \left(\int_0^\tau -\frac{d}{da} \left(\theta(a)^{j-1} \right) e^{(\beta+\gamma)a} da + c[S_k I_j](0) \right)$$
$$= \left(\int_0^\tau -\frac{d}{da} \left(\theta(a)^{j-1} \right) e^{(\beta+\gamma)a} da + \pi(1-\pi) \right) \text{ by substituting initial conditions (2.25).}$$

The groundwork has now been set to extract an expression for $[S_k R_j](\infty)$

Proposition 1.

$$[S_k R_j](\infty) = \left(\frac{\gamma}{\beta+\gamma}\right)\left(\frac{(kp_k)(jp_j)}{\langle k\rangle}\right)\left(1-\theta_\infty^{j-1}\right)\theta_\infty^{(k-1)}$$

Proof. From the calculations above let

$$G_j = F_j e^{-(\beta+\gamma)t} \text{ so that}$$
$$G_j' = F_j' e^{-(\beta+\gamma)t} - (\beta+\gamma)F_j e^{-(\beta+\gamma)t}$$

Noting that

$$F_j' = -\frac{d}{dt}\left(\theta(t)^{j-1}\right)e^{(\beta+\gamma)t}$$

and after integration and substitution

$$\int_0^t G_j' dt = \int_0^t -\frac{d}{dt}\left(\theta(t)^{j-1}\right)dt - \int_0^t (\beta+\gamma)F_j e^{-(\beta+\gamma)t}dt$$

Letting $t \to \infty$ gives

$$G_j(\infty) - G_j(0) = -\theta(t)^{j-1}|_0^\infty - (\beta+\gamma)\int_0^\infty F_j e^{-(\beta+\gamma)t}dt \tag{4.7}$$

$$0 = 1 - \theta_\infty^{j-1} - (\beta+\gamma)\int_0^\infty F_j e^{-(\beta+\gamma)t}dt \tag{4.8}$$

To see why the left hand side is essentially zero requires a bit of work. First note that $G_j(0) \approx 0$ follows immediately from the fact that $F_j(0) \approx 0$ for small enough π. To see why $G_j(\infty) = 0$, we must consider two cases; F_j' is positive, thus F_j either converges to some value or diverges to positive infinity. In the first case it easily follows that

$$\lim_{t\to\infty} G_j = 0$$

In the second case, we apply L'Hôpital's rule, which gives

$$\lim_{t\to\infty} G_j = \lim_{t\to\infty} \frac{\frac{dF_j}{dt}}{(\beta+\gamma)e^{(\beta+\gamma)t}} \tag{4.9}$$

$$= \lim_{t\to\infty} \frac{-\frac{d}{dt}\left(\theta(t)^{j-1}\right)}{(\beta+\gamma)} \tag{4.10}$$

$$= 0 \text{ given by (2.29) (since } \frac{d}{dt}\theta(t) \to 0 \text{ as } t \to \infty)$$

From (4.8) we now have that

$$\frac{1-\theta_\infty^{j-1}}{(\beta+\gamma)} = \int_0^\infty F_j e^{-(\beta+\gamma)t}dt \tag{4.11}$$

By substituting (4.11) into (4.7) gives

$$[S_k R_j](\infty) = \left(\frac{(kp_k)(jp_j)}{\langle k\rangle}\right)\left(\frac{\gamma}{\beta+\gamma}\right)(1-\theta_\infty^{j-1})\theta_\infty^{(k-1)} \tag{4.12}$$

□

Proposition 2.

$$[R_k R_j](\infty) = \frac{jp_j kp_k}{\Psi'(1)}\left(1 - \left(\frac{\gamma}{\beta+\gamma}\right)\left[(1-\theta_\infty^{j-1})\theta_\infty^{k-1} + (1-\theta_\infty^{k-1})\theta^{j-1}\right] - \theta_\infty^{k+j-2}\right)$$

Proof. $[R_k R_j](\infty) = [N_k N_j](\infty) - [S_k R_j](\infty) - [R_k S_j](\infty) - [S_k S_j](\infty)$. The Configuration model assumption gives that $[N_k N_j] = \frac{kp_k jp_j}{\psi'(1)}$; thus, substituting the result from Proposition 1 gives the required result. □

The result of this section is summarized in Table 4.1.

Limiting Values	**How to compute**
$S_k(\infty)$	$p_k\theta_\infty^k$
$A_k(\infty)$	$p_k(1-\theta_\infty^k)$
$[S_j S_k](\infty)$	$\frac{jp_j kp_k \theta_\infty^{k+j-2}}{\Psi'(1)}$
$[S_j R_k](\infty)$	$\left(\frac{\gamma}{\beta+\gamma}\right)\frac{kp_k jp_j(1-\theta_\infty^{j-1})\theta_\infty^{k-1}}{\Psi'(1)}$
$[R_j R_k](\infty)$	$\frac{jp_j kp_k}{\Psi'(1)}\left(1-\left(\frac{\gamma}{\beta+\gamma}\right)\left[(1-\theta_\infty^{j-1})\theta_\infty^{k-1} + (1-\theta_\infty^{k-1})\theta_\infty^{j-1}\right] - \theta_\infty^{k+j-2}\right)$

Table 4.1: Novel expressions for the final state of the network SIR pairwise model. They are given in terms of θ_∞ and degree distribution parameters.

4.3 Second wave network SAIR model

With the full final state for the first wave system, we are ready for the second wave SAIR network model. At the start of the second wave, the recovered individuals in R_k, are susceptible to re-infection again; we label these individuals as A_k. The susceptibility of these individuals is reduced by a factor $\sigma \in [0,1]$. Individuals in S_k remain in S_k. Figure 4.2 shows the possible state class transitions. From the final state of the first wave the second wave variables have initial conditions (with no disease present) $S_k(0) = p_k\theta_\infty^k$, $A_k(0) = p_k(1-\theta_\infty^k)$.

Next, we derive the SAIR network model analogously to the model derived in [25]. The probability that an individual initially in S_k remains susceptible by time t, is the probability that the disease has not been transmitted across any of its k edges. We define θ_{S_k} as the probability that the disease has not been transmitted across an edge that leads to an S_k node at time t. A random network generated by the Configuration

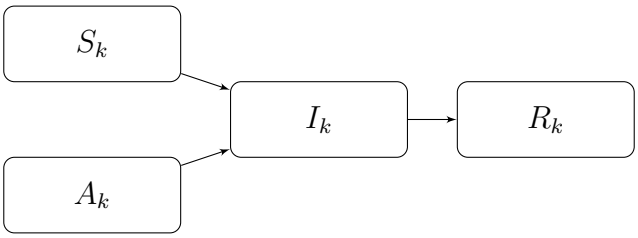

Figure 4.2: State class transitions for degree k nodes in the dynamics for the second wave. Here S_k denotes the fraction of degree k nodes that escaped infection in the first wave and have not been infected in the second wave. A_k is the fraction of degree k nodes that were infected and recovered in the first wave but have not been infected in the second wave.

Model has negligible clustering, thus edges are independent and the probability that a node in S_k is susceptible at time t is $\theta_{S_k}^k$. Define θ_{A_k} in a similar fashion and thus the probability an individual in A_k remains susceptible by time t is $\theta_{A_k}^k$. We define ϕ_{S_k}, ϕ_{A_k} as the fraction of edges leading to a S_k, A_k node and also connected to an infectious node at time t. Note that these edges are also in θ_{S_k} and θ_{A_k}, respectively. Hence,

$$\frac{d}{dt}\theta_{S_k} = -\beta\phi_{S_k} \tag{4.13}$$

$$\frac{d}{dt}\theta_{A_k} = -\sigma\beta\phi_{A_k} \tag{4.14}$$

The dynamical equations for ϕ_{S_k}, ϕ_{A_k} are required. We let h_{S_k} be the probability the node reached following a θ_{S_k} edge (out of the S_k node) has not been infected at time t. Whether or not the neighbour reached is infectious or not depends on its degree and class (whether it is in A or S to begin with). The proportion of edges in θ_{S_k} that lead to a node in S_j is equal to the proportion of edges leading to a node in S_j at the beginning of the second wave, $\frac{[S_k S_j](\infty)}{kS_k}$ multiplied by the probability that the node remains in S_j, $\theta_{S_j}^{j-1}$. The power $j-1$ comes from the fact the fact that transmission cannot be from the neighbour in S_k. Similarly, the node reached is in A_j with probability $\frac{[S_k R_j](\infty)}{kS_k(\infty)}\theta_{A_j}^{j-1}$. Define $P_{S_k|S_j}(0) := \frac{[S_k S_j](\infty)}{kS_k(\infty)}$ and $P_{A_k|S_j}(0) := \frac{[S_k R_j](\infty)}{S_k(\infty)}$; where Table 4.1 provides these limit values. Finally, summing over the possible degrees gives the total fraction of edges leading a non-infectious neighbour as

$$h_{S_k} = \sum_j (P_{A_j|S_k}(0)\theta_{A_j}^{j-1} + P_{S_j|S_k}(0)\theta_{S_j}^{j-1})$$

Futhermore, we define

$$h_{A_k} = \sum_j (P_{A_j|A_k}(0)\theta_{A_j}^{j-1} + P_{S_j|A_k}(0)\theta_{S_j}^{j-1})$$

analogously. For convenience, Table 4.2 summarizes these calculations. In addition,

Appendix C provides some consistency checks for these correlations. The rate at which edges enter ϕ_{S_k}, is equal in magnitude to the rate at which neighbors reached by following a θ_{S_k} edge become infectious. Thus, ϕ_{S_k} is increased at a rate $-\frac{d}{dt}h_{S_k}(t)$. Furthermore, edges in ϕ_{S_k} leave when transmission occurs across the edge or when the infected node recovers. Since the dynamics for ϕ_{A_k} are similar, the equations for ϕ_{S_k} and ϕ_{A_k} may now be written as

$$\frac{d}{dt}\phi_{S_k} = -(\beta+\gamma)\phi_{S_k} - \frac{d}{dt}h_{S_k}$$

and

$$\frac{d}{dt}\phi_{A_k} = -(\sigma\beta+\gamma)\phi_{A_k} - \frac{d}{dt}h_{A_k}$$

Thus,

$$\frac{d}{dt}\phi_{S_k} = -(\beta+\gamma)\phi_{S_k} + \sum_j (j-1)\big(\sigma\beta P_{A_j|S_k}(0)\theta_{A_j}^{j-2}\phi_{A_j} + \beta P_{S_j|S_k}(0)\theta_{S_j}^{j-2}\phi_{S_j}\big) \tag{4.15}$$

$$\frac{d}{dt}\phi_{A_k} = -(\sigma\beta+\gamma)\phi_{S_k} + \sum_j (j-1)\big(\sigma\beta P_{A_j|A_k}(0)\theta_{A_j}^{j-2}\phi_{A_j} + \beta P_{S_j|A_k}(0)\theta_{S_j}^{j-2}\phi_{S_j}\big) \tag{4.16}$$

with initial conditions:

$$\theta_{S_k}(0) = \theta_{A_k}(0) = 1 \tag{4.17}$$

$$\phi_{S_k}(0) = \phi_{A_k}(0) \approx 0 \tag{4.18}$$

We remark that these initial conditions may be interpreted as uniformity in the distribution of initial nodes infected among all network nodes. Note that $P_{A_j|S_k}(0)$ and $P_{S_j|S_k}(0)$ do not depend on k (See Table 4.2), therefore, the equations for ϕ_{S_k} are identical for every k. Thus we drop the subscript k on $P_{A_j|S_k}(0), P_{S_j|S_k}(0), \phi_{S_k}$. The basic reproductive number for this system can be computed as the spectral radius of the next generation matrix [36]. That is

$$\mathcal{R}_0^{(2)} = \rho(FV^{-1}) \tag{4.19}$$

where we order the variables associated with disease states as $\{\phi_{A_1}, \phi_{A_2}, ..\phi_{A_n}, \phi_S\}$ from (4.16) and (4.15). Thus, the F and V^{-1} matrices are $(n+1)\times(n+1)$ with

$$V^{-1} = diag\left(\frac{1}{\sigma\beta+\gamma}, \ldots, \frac{1}{\sigma\beta+\gamma}, \frac{1}{\beta+\gamma}\right)$$

and

$$F = \begin{pmatrix} 0 & \sigma\beta P_{A_2|A_1}(0) & \dots & (n-1)\sigma\beta P_{A_n|A_1}(0) & \beta\sum_j (j-1)P_{S_j|A_1}(0) \\ 0 & \sigma\beta P_{A_2|A_2}(0) & \dots & (n-1)\sigma\beta P_{A_n|A_2}(0) & \beta\sum_j (j-1)P_{S_j|A_2}(0) \\ 0 & \sigma\beta P_{A_2|A_3}(0) & \dots & (n-1)\sigma\beta P_{A_n|A_3}(0) & \beta\sum_j (j-1)P_{S_j|A_3}(0) \\ \vdots & \vdots & & \vdots & \vdots \\ 0 & \sigma\beta P_{A_2|S}(0) & \dots & (n-1)\sigma\beta P_{A_n|S}(0) & \beta\sum_j (j-1)P_{S_j|S}(0) \end{pmatrix}$$

Hence FV^{-1} is

$$\begin{pmatrix} 0 & \frac{\sigma\beta}{\sigma\beta+\gamma} P_{A_2|A_1}(0) & \dots & (n-1)\frac{\sigma\beta}{\sigma\beta+\gamma} P_{A_n|A_1}(0) & \sum_j \frac{\beta}{\beta+\gamma}(j-1)P_{S_j|A_1}(0) \\ 0 & \frac{\sigma\beta}{\sigma\beta+\gamma} P_{A_2|A_2}(0) & \dots & (n-1)\frac{\sigma\beta}{\sigma\beta+\gamma} P_{A_n|A_2}(0) & \sum_j \frac{\beta}{\beta+\gamma}(j-1)P_{S_j|A_2}(0) \\ 0 & \frac{\sigma\beta}{\sigma\beta+\gamma} P_{A_2|A_3}(0) & \dots & (n-1)\frac{\sigma\beta}{\sigma\beta+\gamma} P_{A_n|A_3}(0) & \sum_j \frac{\beta}{\beta+\gamma}(j-1)P_{S_j|A_3}(0) \\ \vdots & \vdots & & \vdots & \vdots \\ 0 & \frac{\sigma\beta}{\sigma\beta+\gamma} P_{A_2|S}(0) & \dots & (n-1)\frac{\sigma\beta}{\sigma\beta+\gamma} P_{A_n|S}(0) & \sum_j \frac{\beta}{\beta+\gamma}(j-1)P_{S_j|S}(0) \\ & & & & \end{pmatrix}$$

with the conditional probabilities given in Table 4.2. Note that from this matrix, $\mathcal{R}_0^{(2)}$ is a function of σ.

Second wave	**How to compute**
$P_{S_j\|A_k}(0)$	$\left(\frac{\gamma}{\beta+\gamma}\right)\frac{jp_j(1-\theta_\infty^{k-1})\theta_\infty^{j-1}}{(1-\theta_\infty^k)\psi'(1)}$
$P_{A_j\|S_k}(0)$	$\left(\frac{\gamma}{\beta+\gamma}\right)\frac{jp_j(1-\theta_\infty^{j-1})}{\theta_\infty\psi'(1)}$
$P_{A_j\|A_k}(0)$	$\frac{jp_j}{(1-\theta_\infty^k)\psi'(1)}\left(1-\left(\frac{\gamma}{\beta+\gamma}\right)\left[(1-\theta_\infty^{j-1})\theta_\infty^{k-1}+(1-\theta_\infty^{k-1})\theta_\infty^{j-1}\right]-\theta_\infty^{k+j-2}\right)$
$P_{S_j\|S_k}(0)$	$\frac{\theta_\infty^{j-2}jp_j}{\psi'(1)}$

Table 4.2: The correlations induced by first wave dynamics are summarized here. $P_{X_j|Y_k}$ may be interpreted as the probability a neighbour of a Y_k node is in X_j. Appendix C provides a few consistency checks for this table.

4.4 A simplification for the network SAIR model

If the correlations induced by the first wave are ignored then the SAIR model simplifies because at the beginning of the second wave the distribution of neighbours for any

node is proportional on their density and degree. Specifically,

$$P_{S_j|A_k}(0) = P_{S_j|S_k}(0) = \frac{jS_j(0)}{\psi'(1)} \tag{4.20}$$

$$P_{A_j|A_k}(0) = P_{S_j|S_k}(0) = \frac{jA_j(0)}{\psi'(1)} \tag{4.21}$$

The independence from subscript k along with uniformity in initial conditions lead to a system of four differential equations that describes the second wave dynamics.

$$\frac{d}{dt}\theta_S = -\beta\phi_S \tag{4.22}$$

$$\frac{d}{dt}\theta_A = -\sigma\beta\phi_A \tag{4.23}$$

$$\frac{d}{dt}\phi_S = -(\beta+\gamma)\phi_S + \sum_j \frac{j(j-1)}{\psi'(1)}\left(\beta S_j(0)\theta_S^{j-2}\phi_S + \sigma\beta A_j(0)\theta_A^{j-2}\phi_A\right) \tag{4.24}$$

$$\frac{d}{dt}\phi_A = -(\sigma\beta+\gamma)\phi_S + \sum_j \frac{j(j-1)}{\psi'(1)}\left(\beta S_j(0)\theta_S^{j-2}\phi_S + \sigma\beta A_j(0)\theta_A^{j-2}\phi_A\right) \tag{4.25}$$

The next generation matrix (FV^{-1}) is rank one and the $\mathcal{R}_0^{(2)} = trace(FV^{-1})$. Thus, for this simplified model,

$$\mathcal{R}_0^{(2)} = \left(\frac{\beta}{\beta+\gamma}\right)\frac{\theta_\infty^2\psi''(\theta_\infty)}{\psi'(1)} + \left(\frac{\sigma\beta}{\sigma\beta+\gamma}\right)\left(\frac{\psi''(1)-\theta_\infty^2\psi''(\theta_\infty)}{\psi'(1)}\right) \tag{4.26}$$

4.5 Numerical results and key new insights

Thus far we have constructed the framework to model the first wave and second wave for a novel influenza strain for all infectious contact structures assumptions considered in this thesis. The fundamental question we are seeking to answer in this thesis is what effect if any does population structure have in the establishment of a pandemic subtype. In other words, once the pandemic wave is extinguished, and values for $\mathcal{R}_0^{(1)}$ are estimated, how much antigenic drift is necessary before a recurrence is possible. The complicated expressions for $\mathcal{R}_0^{(2)}$ require a numerical approach. As in chapter 3, we fix $\mathcal{R}_0^{(1)}$ at 2, and choose a timescale so that $\gamma = 1$ to plot $\mathcal{R}_0^{(2)}$ versus σ (note that once a distribution is set the models are fully and uniquely parametrized). Furthermore, we consider three distribution families

among all models: Poisson, discrete exponential and truncated power law. Note that for multigroup models, the distribution relates to the contact rates among distinct individuals, while for the contact network models, it relates to the total number of contacts an individual has. Figure 4.3 shows that for lower average excess degrees, $\mathcal{R}_0^{(2)}$ for network models increases non-linearly while the random mixing models show a linear increase. This indicates that a recurrence is possible on contact networks at much lower levels of antigenic drift in the time period between the pandemic and the next influenza season. This effect can be dramatic; for example as Figure 4.3 indicates, for networks with average excess degree equal to 3, network models require about 1/4 to 1/2 less antigenic drift for a recurrence than the multigroup and homogeneous models. Of course, in practice, $\mathcal{R}_0^{(1)}$ is an estimate with varying degrees of accuracy, thus Figure 4.4 shows the plots of σ_T versus for $\mathcal{R}_0^{(1)}$ in the range of [1.5, 2.5]. Recall that σ_T is the threshold value for σ so that $\mathcal{R}_0^{(2)} = 1$; i.e., a recurrence is possible. Furthermore, Figure 4.4 suggests that the susceptibility to a recurrence event for network models holds true for a range of $\mathcal{R}_0^{(1)}$ values and in fact tends to increase linearly as $\mathcal{R}_0^{(1)}$ increases. In other words, on a contact network following the initial pandemic, a smaller amount of antigenic drift may be necessary for the first recurrence of the pandemic subtype. Furthermore, from the numerics, the spread among σ_T values models narrows as the average excess degree is increased. This indicates that the contact structure becomes less relevant for predicting a recurrence for networks with large average excess degrees. This appears to be consistent with the result in Appendix A of [25] where it is shown that as the number of contacts every individual has is increased, the dynamics for homogeneous and edge based SIR compartmental models converge. Since increasing the average excess degree increases the expected number of contacts, a convergence to the homogeneous model line is to be expected. We summarize how the computations are done in Table 4.3.

Model	$\mathcal{R}_0^{(1)}$	$\mathcal{R}_0^{(2)}$
Homogeneous	Theorem 1	equation (3.1)
Multigroup	Theorem 3	equation (3.2)
Network	equation (4.1)	spectral radius problem (see eqn. (4.19))
Simplified network	equation (4.1)	equation (4.26)

Table 4.3

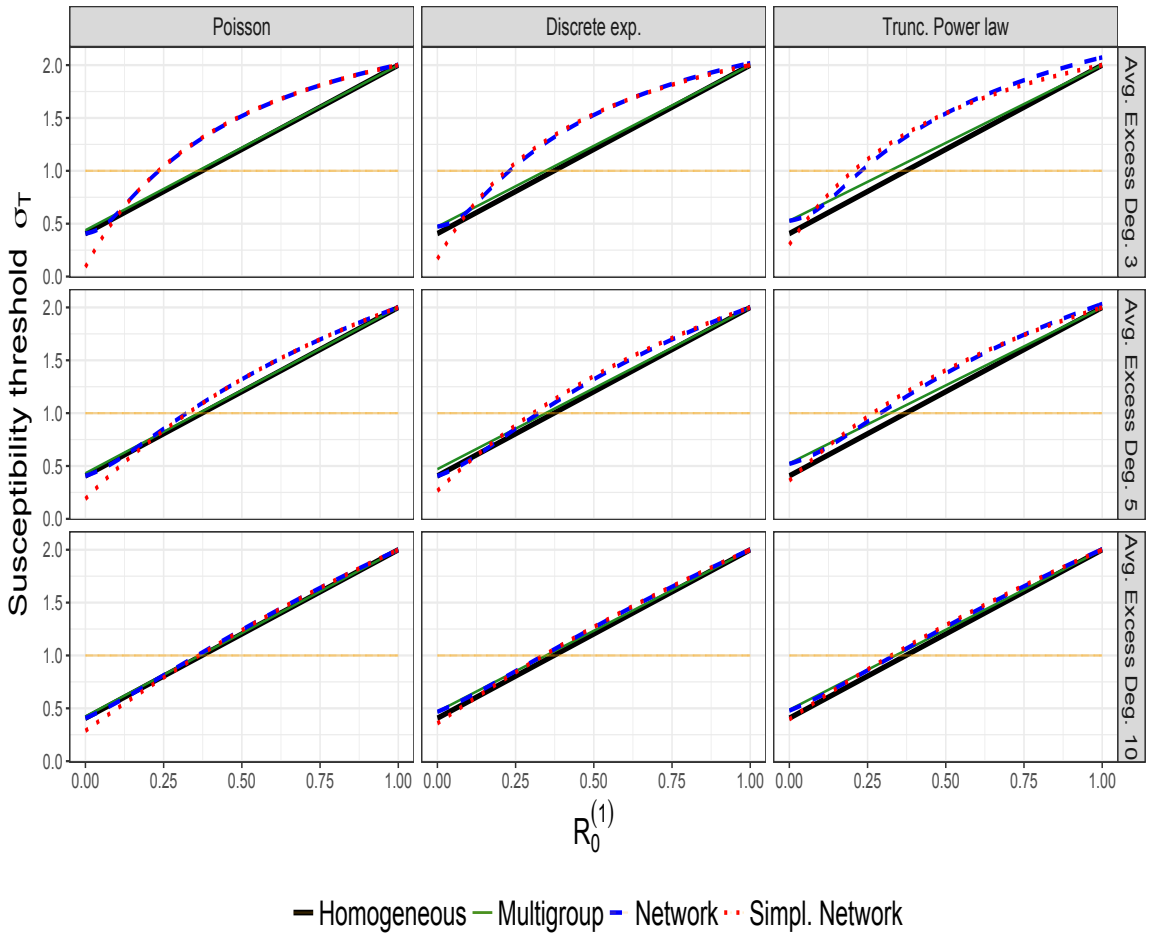

Figure 4.3: As in Figure 3.1 of Chapter 3, $\mathcal{R}_0^{(2)}$ is plotted against susceptibility (σ). Here, $\mathcal{R}_0^{(1)} = 2$ and a timescale has been chosen so that $\gamma = 1$. For network models and and a degree distribution with a low average excess degree, $\mathcal{R}_0^{(2)}$ increases non-linearly with σ; this leads to $\mathcal{R}_0 > 1$ at significantly lower levels of σ when compared to random mixing models. As the average excess degree increases (down a column), all models approach the values for the homogeneous SIR model. Note that the network and simplified network show good agreement

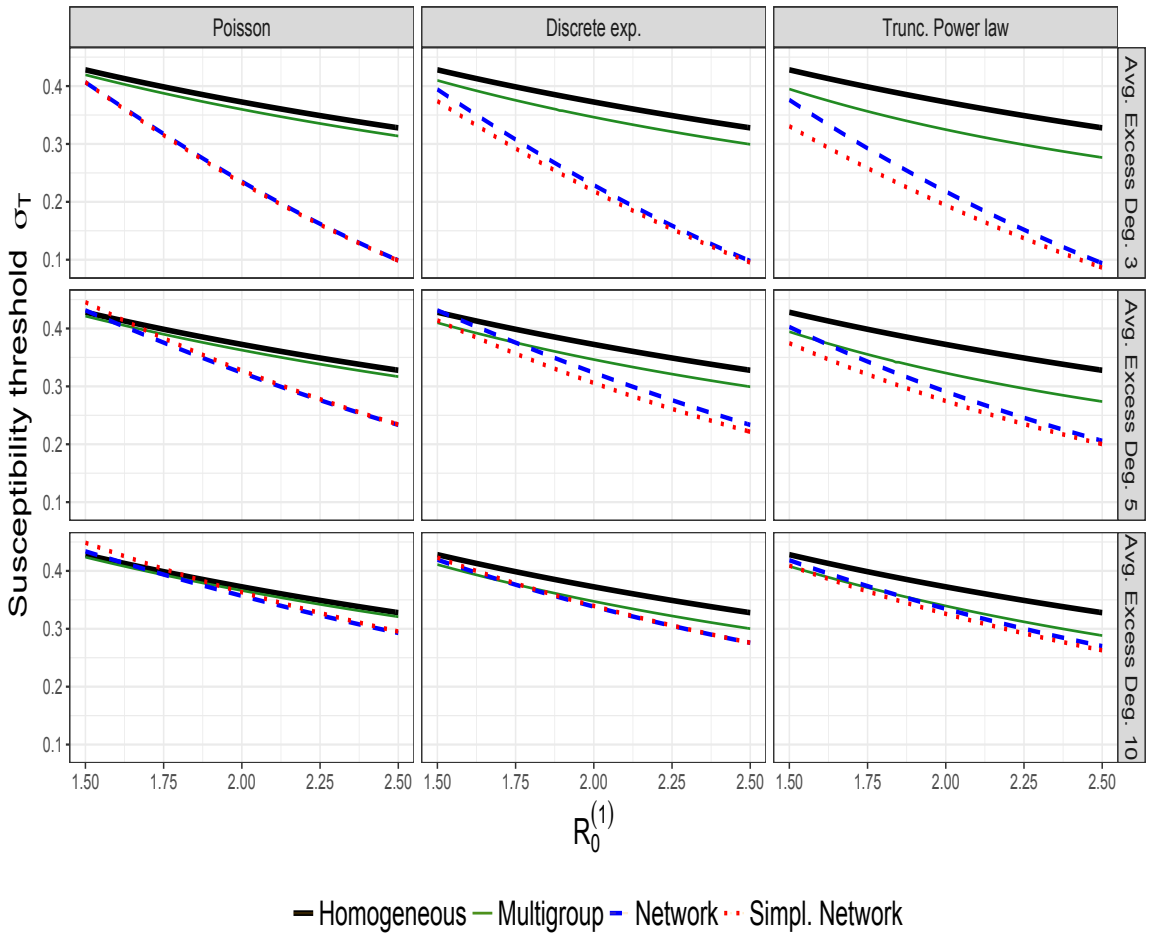

Figure 4.4: As in Figure 3.2 of Chapter 3, we plot the susceptibility threshold (σ_T) versus. $\mathcal{R}_0^{(1)}$. Here, we include the network models along with the random mixing models. In general, σ_T is lower for network models than the random mixing models for a wide range of $\mathcal{R}_0^{(1)}$ values. The gap increases with either increasing $\mathcal{R}_0^{(1)}$ or lowering the average excess degree.

Chapter 5

Discussion and Conclusion

5.1 Discussion

Infectious disease modellers are often faced with the challenge of deciding which features to include and which to exclude in formulating a model. If too many simplifying assumptions are made, then the model might fail to produce accurate results representing reality. On the other hand, including too many features and the model might become intractable and any meaningful insight may be too difficult to extract. Such insight might include optimal control strategies; see, for example, [12, 18] or fundamental biological and ecological results; see, for example, [10, 31].

In this thesis we have shown that host population structure is an important feature to include in influenza models with implications for both control and evolutionary theory of influenza A. Specifically, for contact networks with a low average excess degree, a variant of a particular pandemic influenza A subtype is able to cause a recurrence following modest levels of antigenic drift. This is a result not expected from random mixing models even when heterogeneity in the number of contacts among individuals is considered. In fact, we showed that the linear dependence between $\mathcal{R}_0^{(2)}$ and susceptibility requires an unrealistically large amount of antigenic drift for a recurrence of a novel influenza strain to be possible. From this result, a natural question arises: in biological terms, what causes the dramatic difference in σ_T between network and random mixing models? Although at this point we do not have a satisfactory answer, we can immediately dismiss some hypotheses. These are:

- The correlations induced by the first wave are the main reason why a recurrence is possible at lower levels of susceptibility. Thus, the breaking and forming of

contacts between the first and second wave will do away with this effect.

- For equal $\mathcal{R}_0^{(1)}$ values, network models tend to have a smaller final size when compared to random mixing models. With a smaller fraction of the population infected during the first wave, it immediately follows that less susceptibility is required for a recurrence. Thus, once the models are calibrated so that the final sizes are equal, the effect will diminish.

From our study of the simplified network model, the reader may immediately rule out the first one. Recall that the simplified model assumes that a complete rewiring occurs between the pandemic and second wave. Based on the curves for Figure 4.4, the breaking and forming of contacts in the time after the pandemic and before the second wave begins results in an earlier recurrence for a network with the truncated power law degree distribution.

The second hypothesis is also readily dismissed since it has been shown that for equal $\mathcal{R}_0^{(1)}$ values, SIR epidemics on a network with a Poisson degree distribution satisfes the same final size equation as the homogeneous model [8]. As Figure 4.4 shows, even for a network with a Poisson degree distribution, the reduction in σ_T from the homogeneous or multigroup model can be large. Furthermore, we note that the correlations induced by the first wave dynamics seem to be related to the complexities involved with modelling SIS dynamics on contact networks. Specifically, the case for correlations occurring between recovered and susceptible individuals at the end of and epidemic suggests that the correlations may also emerge during the SIS dynamics.

Finally we note that the curves in Figures 4.3 and 4.4 for the simplified and full network model quantitatively and qualitatively agree well. Thus, this suggests that the simplified network model may be used to study a season-to-season mapping of influenza A as done in [6].

There are however some caveats to consider. First, the modelling framework requires a large population size and a dominant pandemic subtype for the pandemic event. This is in fact the case for New York State in the 2009 H1N1 pandemic, where a single viral lineage was responsible for the majority of confirmed cases [28]. However, in cases where there is no clear dominant strain in the pandemic wave, then this network model framework may not be applicable, or a more homogeneous subpopulation must be considered. Furthermore, our framework assumes negligible clustering and thus in a population that is highly clustered this approach may not

be directly applicable. However, clustering and other effects may be incorporated into network models using, for example, the techniques in [19]. Finally, although not explicitly used in the derivation for the second wave SAIR network model in Chapter 4, it requires triple closure approximations as shown in Appendix B. There is no rigorous justification for these closures and they are possibly responsible for non perfect agreement between $\mathcal{R}_0^{(1)}$ and $\mathcal{R}_0^{(2)}$ when $\sigma = 1$ as shown in Figure 4.3 for the truncated power law distributions with average excess degree 3.

5.2 Conclusion

The purpose of this thesis was to explore how incorporating realistic contact network structures into influenza models may add to our biological and epidemiological understanding for influenza A. Towards this goal we developed a framework that allowed direct comparison between classical random mixing models and network models. Furthermore, for the development of the analytical second wave SAIR network model, we extracted novel correlations induced by the first wave dynamics and also considered a simpler network model with no correlations. Our analysis revealed that generally, for network models recurrence may occur at modest antigenic drift levels while random mixing models predict otherwise. This contributes the growing body of evidence that suggest incorporating contact network structures into disease models is important. Specifically, here we found that relatively fixed pool of contacts such as family members, classmates, and co-workers among whom the spread of influenza is restricted, may be crucial for the spread of influenza in human populations.

Appendix A

From full pairwise SIR to EBCM SIR model

In Chapter 2, we presented a derivation for the Miller model from first principles. Here we show how under the right initial conditions, the full pairwise SIR leads to the Miller model [26]. These results are well documented however, we provide them here for completeness. Bridging the two models yields some new results for the final state of the pairwise model.

Recall that the full pairwise SIR model is fully described by the equations (2.21)-(2.24) and initial conditions (2.25)-(2.28). Note that these initial conditions represent the scenario where initially infectious individuals are selected at random from the population. As shown next, this assumption is key in arriving at the Miller model.

Define higher order variables from the first wave dynamical variables. For node classes, $\{S_k, S_j\}$, let

$$P_{S_k|S_j} := \frac{[S_k S_j]}{jS_j} \tag{A.1}$$

This variable may be interpreted as the proportion of edges arriving at a susceptible node of degree k, given that the edge starts at a susceptible node of degree j.. We define $P_{S_k|R_j}, P_{R_k|S_j}, P_{R_k|R_j}$ similarly. The dynamical equations for $P_{S_k|S_j}$ are now derived using (2.22) and (2.24).

$$\frac{d}{dt}P_{S_k|S_j} = \beta P_{S_k|S_j} P_{I|S_j} - \beta(k-1)P_{I|S_k}P_{S_k|S_j} \tag{A.2}$$

Equation (A.2) is linear in $P_{S_k|S_j}$ and the solution is given by

$$P_{S_k|S_j} = P_{S_k|S_j}(0)e^{-\beta\int_0^t((k-1)P_{I|S_k}-P_{I|S_j})dt} \tag{A.3}$$

Let

$$\theta_k := e^{-\beta\int_0^t P_{I|S_k}dt} \tag{A.4}$$

to simplify equation (A.3)

$$P_{S_k|S_j} = P_{S_k|S_j}(0)\theta_k^{k-1}\theta_j^{-1} \tag{A.5}$$

Note that θ_k requires the dynamic variable $P_{I|S_k}$ Thus, we derive the dynamical equation for $P_{I|S_k}$ as follows.

$$\begin{aligned}
P_{I_j|S_k} &= \frac{[S_kI_j]}{kS_k} \qquad (A.6)\\
\frac{d}{dt}P_{I_j|S_k} &= \frac{\frac{d}{dt}[S_kI_j]}{kS_k} - \frac{[S_kI_j]}{k(S_k)^2}(\frac{d}{dt}S_k)\\
&= -\beta\frac{[S_kI_j]}{kS_k} + \beta\frac{[S_kS_j][S_jI](j-1)}{(kS_k)(jS_j)} - \beta\frac{[I_jS_k][S_kI](k-1)}{k(S_k)^2} - \gamma\frac{[S_kI_j]}{kS_k} - \frac{[S_kI_j]}{k(S_k)^2}\frac{d}{dt}S_k\\
&= -\beta P_{I_j|S_k} + \beta P_{S_j|S_k}P_{I|S_j}(j-1) - \beta P_{I_j|S_k}P_{I|S_k}(k-1) - \gamma P_{I_j|S_k} + k\beta P^2_{I_j|S_k}\\
&= -\beta P_{I_j|S_k} + \beta P_{S_j|S_k}P_{I|S_j}(j-1) - \gamma P_{I_j|S_k} + \beta P^2_{I_j|S_k}
\end{aligned}$$

Since

$$\begin{aligned}
&\frac{d}{dt}P_{I|S_k} = \sum\frac{d}{dt}P_{I_j|S_k} \text{ then,}\\
&\frac{d}{dt}P_{I|S_k} = -\beta P_{I|S_k} + \sum_j \beta P_{S_j|S_k}P_{I|S_j}(j-1)) - \gamma P_{I|S_k} + \beta P^2_{I|S_k} \qquad (A.7)
\end{aligned}$$

Substituting (A.5) into equation (A.7) gives

$$P'_{I|S_k} = -(\beta+\gamma)P_{I|S_k} + \theta_k^{-1}\sum_j \beta P_{S_j|S_k}(0)\theta_j^{j-1}P_{I|S_j}(j-1) + \beta P^2_{I|S_k} \tag{A.8}$$

At this point we make the following observations: the dynamical equations for $P_{I|S_k}, P_{I|S_\ell}$ are identical and thus if $P_{S_j|S_k}(0) = P_{S_j|S_\ell}(0)$ and $P_{I|S_k}(0) = P_{I|S_\ell}(0)$, it follows that $P_{I|S_k}(t) = P_{I|S_\ell}(t)$ for all t. Recall that the initial assumptions made earlier along with the Configuration Model framework guarantee these initial condi-

tions. Therefore, $\theta_k = \theta_\ell$ from definition (A.4) and we drop the subscript k from $P_{S_j|S_k}, P_{I|S_k}, \theta_k$ in future use. In particular, note that equations (A.5), (A.4), (A.8) become

$$\theta = e^{-\beta \int_0^t P_{I|S} d\tau} \tag{A.9}$$

$$P_{S_k|S}(t) = P_{S_k|S_j}(0)\theta^{k-2} \tag{A.10}$$

and

$$P'_{I|S} = -(\beta+\gamma)P_{I|S} + \theta^{-1}\sum_j \beta(j-1)P_{S_j|S}(0)\theta^{j-1}P_{I|S} + \beta P_{I|S}^2 \tag{A.11}$$

respectively, We divert briefly to point out a direct result that will be of particular use to us. Taking (A.1), (A.10) combined with the fact $S_k = p_k\theta^k$ [25], gives

$$[S_k S_j](t) = \frac{(kp_k)(jp_j)\theta^{k+j-2}}{\psi'(1)} \tag{A.12}$$

Since θ_∞ is numerically simple to calculate, it follows that the final state $[S_k S_j](\infty)$ is straightforward to calculate as well. Continuing with the derivation of the Miller model, we define the new variable $\phi := \theta P_{I|S}$. The choice of this notation is appropriate for as we show next, it is equivalent to the ϕ that appears in [25]. Computing the derivative for ϕ gives

$$\phi' = \theta' P_{I|S} + \theta P'_{I|S} \tag{A.13}$$

Substituting (A.1), (A.11), (A.9) along with (2.25)-(2.28) into (A.14) and some simplification gives

$$\phi' = -(\beta+\gamma)\phi + \beta\frac{\psi''(\theta)}{\psi'(1)}\phi \tag{A.14}$$

Thus we have recovered the equations for θ and ϕ found in [25]. However, θ and ϕ are meaningless unless they can be used to recover epidemiological quantities of interest such as S. Using (2.19) and (A.8), yields the ODE

$$S'_k = -k\beta S_k P_{I|S_k} = -k\beta S_k P_{I|S} \tag{A.15}$$

This ODE is linear in S_k, thus solving it and substituting (A.9) gives $S_k = S_k(0)\theta^k$. Finally, using (2.25) and summing over k gives $S = \sum p_k\theta^k = \psi(\theta)$ as required.

Appendix B

From full pairwise SAIR to EBCM SAIR model

The system up to the level of triples is:

$$\frac{d}{dt}[S_k] = -\beta[S_k I] \tag{B.1}$$

$$\frac{d}{dt}[A_k] = -\sigma\beta[A_k I] \tag{B.2}$$

$$\frac{d}{dt}[S_k S_j] = -\beta\left([I S_k S_j] + [S_k S_j I]\right) \tag{B.3}$$

$$\frac{d}{dt}[A_k A_j] = -\sigma\beta\left([I A_k A_j] + [A_k A_j I]\right) \tag{B.4}$$

$$\frac{d}{dt}[S_k A_j] = -\beta\left([I S_k A_j] + \sigma[S_k A_j I]\right) \tag{B.5}$$

$$\frac{d}{dt}[S_k I_j] = -\beta\left([S_k I] + [I S_k I_j]\right) + \beta\left(\sigma[S_k A_j I] + [S_k S_j I]\right) - \gamma[S_k I_j] \tag{B.6}$$

$$\frac{d}{dt}[A_k I_j] = \beta\left([A_k S_j I] + \sigma[A_k A_j I]\right) - \sigma\beta\left([A_k I_j] + [I A_k I_j]\right) - \gamma[A_k I_j] \tag{B.7}$$

Applying the standard triple closure scheme (2.20) gives

$$\frac{d}{dt}[S_kS_j] = -\beta\left(\frac{[IS_k][S_kS_j](k-1)}{kS_k} + \frac{[S_kS_j][S_jI](j-1)}{jS_j}\right) \tag{B.8}$$

$$\frac{d}{dt}[A_kA_j] = -\beta\left(\frac{[IA_k][A_kA_j](k-1)}{kA_k} + \frac{[A_kA_j][A_jI](j-1)}{jA_j}\right) \tag{B.9}$$

$$\frac{d}{dt}[S_kA_j] = -\beta\left(\frac{[IS_k][S_kA_j](k-1)}{kS_k} + \sigma\frac{[S_kA_j][A_jI](j-1)}{jA_j}\right) \tag{B.10}$$

$$\begin{aligned}\frac{d}{dt}[S_kI_j] =& -(\beta+\gamma)[S_kI_j] - \beta(k-1)\left(\frac{[IS_k][S_kI_j]}{kS_k}\right) + \\ & \beta(j-1)\left(\sigma\frac{[S_kA_j][A_jI]}{jA_j} + \frac{[S_kS_j][S_jI]}{jS_j}\right)\end{aligned} \tag{B.11}$$

$$\begin{aligned}\frac{d}{dt}[A_kI_j] =& -(\sigma\beta+\gamma)[A_kI_j] - \sigma\beta(k-1)\left(\frac{[IA_k][A_kI_j]}{kA_k}\right) + \\ & \beta(j-1)\left(\frac{[A_kS_j][S_jI]}{jS_j} + \sigma\frac{[A_kA_j][A_jI]}{jA_j}\right)\end{aligned} \tag{B.12}$$

We proceed to deriving the equations for (4.16) and (4.13). The work for (4.15) and (4.14) follow analogously. Letting

$$P_{I|S_k} := \frac{[S_kI]}{kS_k} \tag{B.13}$$

$$P_{A_j|S_k} := \frac{[A_jS_k]}{kS_k} \tag{B.14}$$

gives

$$P'_{A_j|S_k} = \beta P_{A_j|S_k}P_{I|S_k} - \sigma\beta P_{A_j|S_k}(j-1)$$

Solving yields

$$P_{A_j|S_k}(t) = P_{A_j|S_k}(0)e^{\beta\int_0^t P_{I|S_k}d\tau}e^{-\sigma\beta(j-1)\int_0^t P_{I|A_k}d\tau} \tag{B.15}$$

$$= P_{A_j|S_k}(0)\theta_{S_k}^{-1}\theta_{A_k}^{j-1} \tag{B.16}$$

where

$$\theta_{S_k} := e^{-\beta \int_0^t P_{I|S_k} d\tau} \tag{B.17}$$

$$\theta_{A_k} := e^{-\sigma\beta \int_0^t P_{I|A_k} d\tau} \tag{B.18}$$

Summing (B.11) over j gives

$$\begin{aligned}[S_k I]' = &-(\beta+\gamma)[S_k I] - P_{I|S_k}[S_k I](k-1)+ \\ &\beta \sum_j \left(P_{I|A_j}[S_k A_j](j-1) + P_{I|S_j}[S_k S_j](j-1)\right)\end{aligned} \tag{B.19}$$

Using (B.13) gives

$$\begin{aligned}P'_{I|S_k} = &-(\beta+\gamma)P_{I|S_k} - \beta P^2_{I|S_k}(k-1)+ \\ &\beta \sum_j \left(P_{I|A_j} P_{A_j|S_k}(j-1) + P_{I|S_j} P_{S_j|S_k}(j-1)\right) + k\beta P^2_{I|S_k}\end{aligned} \tag{B.20}$$

$$\begin{aligned}P'_{I|S_k} = &-(\beta+\gamma)P_{I|S_k} + \beta \sum_j \left(P_{I|A_j} P_{A_j|S_k}(j-1) + P_{I|S_j} P_{S_j|S_k}(j-1)\right) + \\ &\beta P^2_{I|S_k}\end{aligned} \tag{B.21}$$

Now we define the variable

$$\phi_{S_k} := \theta_{S_k} P_{I|S_k} \tag{B.22}$$

so that

$$\phi_{S_k} : = \theta_{S_k} P_{I|S_k} \tag{B.23}$$

$$\phi'_{S_k} = \theta'_{S_k} P_{I|S_k} + \theta_{S_K} P'_{I|S_k} \tag{B.24}$$

$$= -\beta P_{S_k}^2 \theta_{S_k} + \theta_{S_k}(-(\beta+\gamma)P_{I|S_k} + \tag{B.25}$$

$$\tag{B.26}$$

$$\beta\theta_{S_k} \sum_j \left(P_{I|A_j} P_{A_j|S_k}(j-1) + P_{I|S_j} P_{S_j|S_k}(j-1) \right) + \beta P_{I|S_k}^2$$

$$= -(\beta+\gamma)\theta_{S_k} P_{I|S_k} + \beta\theta_{S_k} \sum_j \left(P_{I|A_j} P_{A_j|S_k}(j-1) + P_{I|S_j} P_{S_j|S_k}(j-1) \right) \tag{B.27}$$

$$= -\phi_{S_k}(\beta+\gamma) + \tag{B.28}$$

$$\beta \sum_j \left(P_{A_j|S_k}(0)\theta_{A_j}^{(j-2)} P_{I|A_j} \theta_{A_j}(j-1) + P_{S_j|S_k}(0)\theta_{S_j}^{(j-2)} P_{I|S_j} \theta_{S_j}(j-1) \right)$$

where we have used (B.16). Substituting (B.23) gives

$$= -\phi_{S_k}(\beta+\gamma) + \sum_j \left(P_{A_j|S_k}(0)\theta_{A_j}^{(j-2)} \phi_{A_j}(j-1) + P_{S_j|S_k}(0)\theta_{S_j}^{(j-2)} \phi_{S_j}(j-1) \right) \tag{B.29}$$

as required. Finally note that

$$\frac{d}{dt}\theta_{S_k} = -\beta P_{I|S_k} \theta_{S_k} \tag{B.30}$$

$$= -\beta \phi_{S_k} \tag{B.31}$$

To show that

$$S(t) = \sum S_k(0)\theta_S^k + \sum A_k(0)\theta_{A_k}^k$$

a similar calculation as done in Appendix A is applied.

Appendix C

Correlation consistency checks

We show that at the end of the pandemic, the proportion of neighbours of an S_k node that are in class A or S sums to one. That is,

Proposition 3. $\sum_j P_{A_j|S_k} = 1 - P_{S|S}$

Proof. Using Table 4.2,

$$\begin{aligned}\sum_j P_{A_j|S_k} &= \left(\frac{\gamma}{\gamma+\beta}\right)\left(\frac{1}{\theta_\infty}\right)\left(1-\frac{\Psi'(\theta_\infty)}{\Psi'(1)}\right)\\ &= \left(\frac{1}{\theta_\infty}\right)\left(\frac{\gamma}{\gamma+\beta}\right) - \left(1-\frac{\beta}{\beta+\gamma}\right)\left(\frac{\Psi'(\theta_\infty)}{\Psi'(1)\theta_\infty}\right)\\ &= \left[\left(\frac{1}{\theta_\infty}\right)\left(\frac{\gamma}{\gamma+\beta}+\frac{\beta}{\beta+\gamma}\frac{\Psi'(\theta_\infty)}{\Psi'(1)}\right)\right] - \frac{\Psi'(\theta_\infty)}{\theta_\infty\Psi'(1)}\end{aligned}$$

Invoking the final size equation satisfied by θ_∞ gives

$$\begin{aligned}&= 1 - \frac{\Psi'(\theta_\infty)}{\theta_\infty\Psi'(1)}\\ &= 1 - P_{S|S}\end{aligned}$$

□

Proposition 4. $P_{S_1|S_k} = \frac{\theta_\infty^{-1}p_1}{\langle k\rangle} \leq 1$

Proof. Recall that θ_∞ satisfies the equation

$$\theta_\infty = \frac{\gamma}{\gamma+\beta} + \left(\frac{\beta}{\beta+\gamma}\right)\frac{\psi'(\theta_\infty)}{\psi'(1)} \tag{C.1}$$

Since and ψ is monotonically increasing, $\theta_\infty \geq \frac{\gamma}{\gamma+\beta}$, and from (C.1),

$$\theta_\infty \geq \frac{\gamma}{\gamma+\beta} + \left(\frac{\beta}{\beta+\gamma}\right)\frac{\psi'(\frac{\gamma}{\gamma+\beta})}{\psi'(1)}$$

Expanding out

$$\theta_\infty \geq \frac{\gamma}{\gamma+\beta} + \left(\frac{\beta}{\beta+\gamma}\right)\frac{p_1}{\psi'(1)} + \left(\frac{\beta}{\beta+\gamma}\right)\sum_{k=2}^{N}\frac{kp_k}{\psi'(1)}\left(\frac{\gamma}{\gamma+\beta}\right)^{k-1}$$

Finally, noting that $\frac{p_1}{\psi'(1)} \leq 1$ gives

$$\theta_\infty \geq \left(\frac{\gamma}{\gamma+\beta}\right)\frac{p_1}{\psi'(1)} + \left(\frac{\beta}{\beta+\gamma}\right)\frac{p_1}{\psi'(1)} + \left(\frac{\beta}{\beta+\gamma}\right)\sum_{k=2}^{N}\frac{kp_k}{\psi'(1)}\left(\frac{\gamma}{\gamma+\beta}\right)^{k-1}$$

and the result follows. □

Appendix D

Probability distributions information

In this thesis we focused on three commonly used discrete probability distribution families. They are Poisson, discrete exponential, and truncated power law. Table D.2 gives the general expression for the probability mass function (PMF) and Table D.1 provides a brief summary on the specific parameterizations used. It is important to note that they are chosen to illustrate possible susceptibility threshold (σ_T) values but are not based on any evidence related to influenza A contact networks or rates of contact. Furthermore, many other distribution families were not considered. For more specific studies, an appropriate probability distribution and parametrization thereof should be utilized.

Distribution family	**PMF**
Poisson(λ)	$f(k) = \frac{\lambda^k e^{-k}}{k!}$
Discrete exponential(a)	$f(k) = (1 - e^{-1/a})e^{-k/a}$
Trunc. power law (c, d)	$f(k) = ck^{-1.728}e^{-k*d/40}$

Table D.1: The distribution is specified by family type and specific shape parameters. $f(a) = prob(k = a)$.

Distribution type	**E[k]**	**Var[k]**	$\frac{\langle k^2 \rangle}{\langle k \rangle}$	**Avg. excess degree**	$\frac{\sqrt{Vark}}{E[k]}$
Poisson(3)	3.0	3.0	4.0	3.0	0.58
Poisson(5)	5.0	5.0	6.0	5.0	0.45
Poisson(10)	10	10	11	10	0.32
Discrete exp.(2.0)	1.5	3.8	4.0	3.0	1.3
Discrete exp.(3.0)	2.5	8.7	6.0	5.0	1.2
Discrete exp.(5.6)	5.1	30	11	10	1.1
Trunc. power law(0.74,5.5)	1.9	4.0	4.0	3.0	1.0
Trunc. power law(0.66,3.2)	2.3	8.5	6.0	5.0	1.3
Trunc. power law(0.55,0.50)	3.2	25	11	10	1.5

Table D.2: The specific parameterizations and summary statistics are provided here. For the numerics, the distributions were capped at $k = 40$.

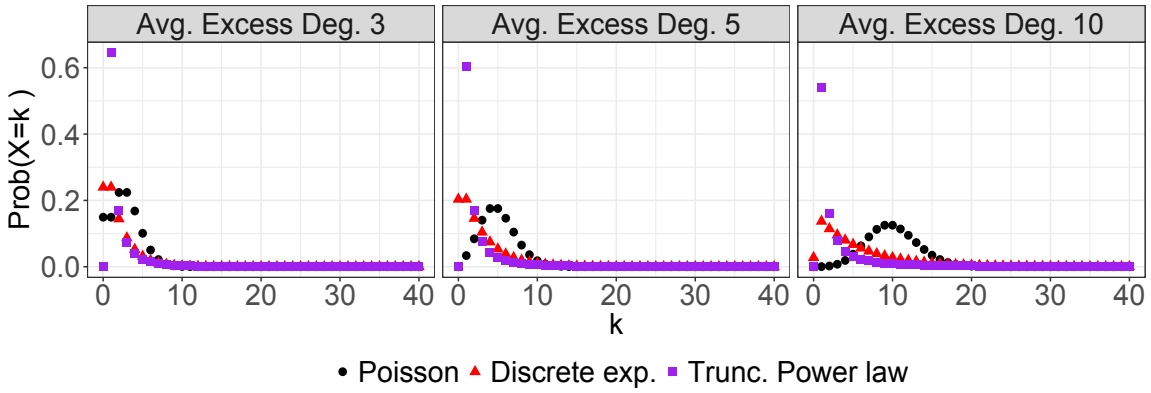

(a)

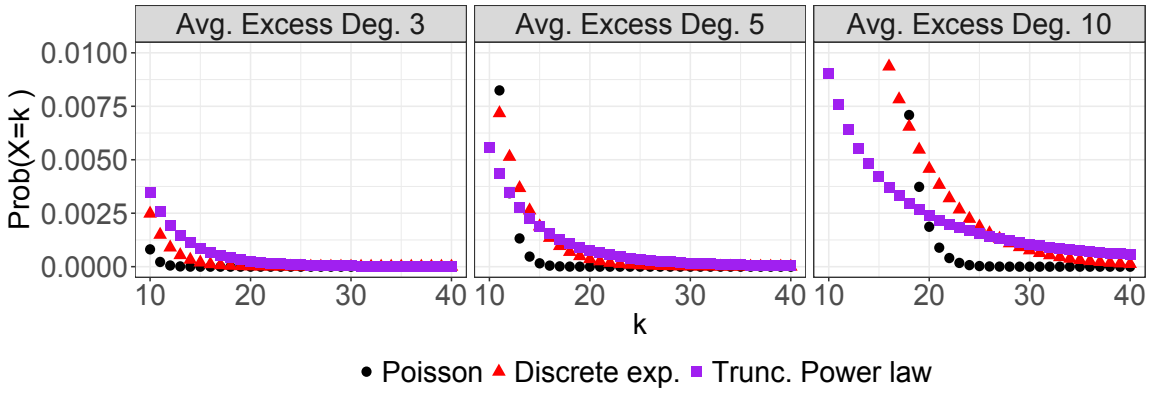

(b)

Figure D.1: Figure D.1 (a) illustrates the PMF $f(k)$ vs. k for each distribution type based on average excess degree. Figure D.1 (b) shows the tail end of the distributions.

Bibliography

[1] World Health Organization. `http://www.who.int/immunization/topics/influenza/en/`, 2008. Immunization, Vaccines and Biologicals: influenza; 2017. Online.

[2] World Health Organization. `http://www.who.int/mediacentre/factsheets/fs211/en/`, 2016. Fact sheet 211: influenza; 2016. Online.

[3] V. Andreasen. Dynamics of annual influenza A epidemics with immuno-selection. *Journal of Mathematical Biology*, 46:504–536, 2003.

[4] V. Andreasen, J. Lin, and S.A. Levin. The dynamics of cocirculating influenza strains conferring partial cross-immunity. *Journal of Mathematical Biology*, 35:825–842, 1997.

[5] S.M. Asaduzzaman, J. Ma, and P. van den Driessche. The coexistence or replacement of two subtypes of influenza. *Mathematical Biosciences*, 270, Part A:1–9, 2015.

[6] M.F. Boni, J.R. Gog, V. Andreasen, and F.B. Christiansen. Influenza drift and epidemic size: the race between generating and escaping immunity. *Theoretical Population Biology*, 65, 2004.

[7] G.W. Both, M.J. Sleigh, N.J. Cox, and A.P. Kendal. Antigenic drift in influenza virus H3 Hemagglutinin from 1968 to 1980: multiple evolutionary pathways and sequential amino acid changes at key antigenic sites. *Journal of Virology*, 48:52–60, 1983.

[8] F. Brauer, P. van den Driessche, and J Wu, editors. *Mathematical epidemiology*, volume 1945. Springer, 2008.

[9] F. Carrat and A. Flahault. Influenza vaccine: The challenge of antigenic drift. *Vaccine*, 25:39–40, 2007.

[10] R. Casagrandi, L. Bolzoni, S.A. Levin, and V. Andreasen. The SIRC model and influenza A. *Mathematical Biosciences*, 200:152–169, 2006.

[11] S. Chatterjee and R. Durrett. Contact processes on random graphs with power law degree distributions have critical value 0. *The Annals of Probability*, 37:2332–2356, 2009.

[12] J.M. Conway, A.R. Tuite, D.N. Fisman, Hupert N., et al. Vaccination against 2009 pandemic H1N1 in a population dynamical model of Vancouver, Canada: timing is everything. *BMC Public Health*, 11:43–56, 2011.

[13] N.J. Cox and K. Subbarao. Global epidemiology of influenza: past and present. *Annual Review of Medicine*, 51:407–421, 2000.

[14] O. Diekmann, J.A.P. Heesterbeek, and J.A.J. Metz. On the definition and the computation of the basic reproduction ratio $\mathcal{R}_0$ in models for infectious diseases in heterogeneous populations. *Journal of Mathematical Biology*, 28:365–382, 1990.

[15] K.T.D. Eames and M.J. Keeling. Modeling dynamic and network heterogeneities in the spread of sexually transmitted diseases. *Proceedings of the National Academy of Sciences*, 99:13330–13335, 2002.

[16] D.J.D. Earn, J. Dushoff, and S.A. Levin. Ecology and evolution of the flu. *Trends in Ecology & Evolution*, 17:334–340, 2017.

[17] S.L. Feld. Why your friends have more friends than you do. *American Journal of Sociology*, 96:1464–1477, 1991.

[18] H.W. Hethcote and J.W. Van Ark. Epidemiological models for heterogeneous populations: proportionate mixing, parameter estimation, and immunization programs. *Mathematical Biosciences*, 84:85 – 118, 1987.

[19] T. House and M.J. Keeling. Insights from unifying modern approximations to infections on networks. *J.R. Soc. Interface*, 8:67 – 73, 2010.

[20] W.O. Kermack and A.G. McKendrick. A contribution to the mathematical theory of epidemics. *Proceedings of the Royal Society of London. Series A*, 115:700–721, 1927.

[21] I.Z. Kiss, J.C. Miller, and P.L. Simon. *Mathematics of epidemics on networks: from exact to approximate models*, volume 46. Springer, 2017.

[22] E.Y. Klein, J.M. Serohijos, A.W.R. Choi, E.I. Shakhnovich, and A. Pekosz. Influenza A H1N1 pandemic strain evolution – divergence and the potential for antigenic drift variants. *PLOS ONE*, 9:1–10, 2014.

[23] A.J. Kucharski, J. Lessler, J.M. Read, H. Zhu, et al. Estimating the life course of influenza A(H3N2) antibody responses from cross-sectional data. *PLOS Biology*, 13:1–16, 2015.

[24] J. Lindquist, J. Ma, P. van den Driessche, and F.H. Willeboordse. Effective degree network disease models. *Journal of Mathematical Biology*, 62:143–164, 2011.

[25] J.C. Miller. A note on a paper by Erik Volz: SIR dynamics in random networks. *Journal of Mathematical Biology*, 62:349–358, 2011.

[26] J.C. Miller and I.Z. Kiss. Epidemic spread in networks: existing methods and current challenges. *Mathematical Modelling of Natural Phenomena*, 9:4–42, 2014.

[27] C.E. Mills, J.M. Robins, and M. Lipsitch. Transmissibility of 1918 pandemic influenza. *Nature*, 432:904–906, 2004.

[28] M.I. Nelson, Y. Tan, et al. Phylogeography of the spring and fall waves of the H1N1/09 pandemic influenza virus in the United States. *Journal of Virology*, 85(2):828–834, 2011.

[29] M.E.J. Newman. The spread of epidemic disease on networks. *Physical Review Letters*, 66, 2002.

[30] R. Pastor-Satorras and A. Vespignani. Epidemic dynamics and endemic states in complex networks. *Physical Review E*, 63, 2001.

[31] C.M. Pease. An evolutionary epidemiological mechanism, with applications to type A influenza. *Theoretical Population Biology*, 31:422–452, 1987.

[32] C.M. Perez, M. Ferres, and J.A. Labarca. Pandemic (H1N1) 2009 reinfection, Chile. *Emerging Infectious Diseases*, 16:156–157, 2010.

[33] C.W. Potter. A history of influenza. *Journal of Applied Microbiology*, 91(4):572–579, 2001.

[34] B. Pourbohloul, L.A Meyers, D.M. Skowronski, M. Krajden, D.M. Patrick, and R.C. Brunham. Modeling control strategies of respiratory pathogens. *Emerging Infectious Diseases*, 11:1249–1256, 2005.

[35] T.J. Taylor and I.Z. Kiss. Interdependency and hierarchy of exact and approximate epidemic models on networks. *Journal of Mathematical Biology*, 69:183–211, 2014.

[36] P. van den Driessche and J. Watmough. Reproduction numbers and subthreshold endemic equilibria for compartmental models of disease transmission. *Mathematical Biosciences*, 180:29–48, 2002.

[37] E. Volz. SIR dynamics in random networks with heterogeneous connectivity. *Journal of Mathematical Biology*, 56:293–310, 2008.